TECHNICAL UNIVERSITY OF CRETE
ELECTRONIC AND COMPUTER ENGINEERING DEPARTMENT
TELECOMMUNICATIONS DIVISION

Implementation of Frequency Division Multiple Access Digital Backscatter Sensor Netwok

by

Konstantinos Tountas

A THESIS SUBMITTED IN PARTIAL FULFILLMENT OF
THE REQUIREMENTS FOR THE DIPLOMA OF

ELECTRONIC AND COMPUTER ENGINEERING

October 2014

THESIS COMMITTEE

Associate Professor Aggelos Bletsas, *Thesis Supervisor*
Associate Professor George N. Karystinos
Associate Professor Antonios Deligiannakis

Abstract

Environmental sensing applications require dense sensor deployments for precise monitoring of each plants' micro-climate; For such applications, scatter radio is a promising communication and networking technology. Since modulation is achieved by means of reflection, very low-cost and low-power RF front-ends and sensor nodes can be constructed. However, such technology has demonstrated limited range in commercial scatter radio applications, like radio frequency identification (RFID) systems. In order to alleviate that problem, the bistatic architecture has been proposed, where emitter of illuminating carrier towards the tag/sensor and reader of the modulated reflection (from tag/sensor) are dislocated. Also, frequency shift keying (FSK) modulation has been utilized for simultaneous transmission of many scatter radio sensors, through frequency division multiple access (FDMA). These schemes allow the creation of a scatter sensor network, using flexible topologies with multiple emitters and a single reader, increasing the probability for short emitter-to-tag/sensor distances. This work experimentally demonstrates the creation of such scatter radio network with low-cost 8051 micro-controller units (MCU), where sensed information is converted to digital messages using the internals analog-to-digital (ADC) converters. Furthermore, implementation of short-block length channel encoding based on Reed-Muller and Golay codes are tested experimentally. This work is a small step towards the realization of large-scale, scatter radio sensor networks.
Thesis Supervisor: Associate Professor Aggelos Bletsas

Acknowledgements

As my undergraduate studies are coming to an end, I must say that the past years have been really important to me. Lots of ups and downs, a lot of work, a lot of fun. Prof. Aggelos Bletsas, was my mentor and was like a father to me. He opened my way in the world of research and everything I know I owe it to him. My dear friends and colleagues J. Kimionis and E. Kampianakis were the people that supported me and guided me throughout my undergraduate studies and I.P. Athanasiou and N. Agadakos are the closest thing I have to brothers. My family supported me and encouraged me every single day. I would like to thank all of them for believing in me. I now start my graduate studies with great experiences and beautiful moments in my mind. The greatest challenges lie ahead.

To my family, my mentor and all those who made my last year special...

Table of Contents

List of Figures

Chapter 1

Introduction

1.1 Large-scale Wireless Sensor Networks

In the modern era observing and protecting the environment has become very important. The unscrupulous exploitation of the planet's natural resources makes the monitoring of the environment and agriculture a necessity. The monitoring will lead to water-saving, forest and wildlife conservation etc. In the last few years farmers have been embracing what is called "precision agriculture". This means that the watering and fertilizing schedules change according to the information about the soil's moisture and minerals and each plant's condition. Using these information correctly results in water-saving and production growth. But typical monitoring technologies have large nodes connected by myriad wires. On the other hand, wireless sensor networks (WSNs) are an important technology for large-scale monitoring, providing sensor measurements at high temporal and spatial resolution, transferring the data wirelessly, utilizing small sized nodes. The WSN nodes are devices utilizing low-cost, low-power, feature-rich microcontrollers with analog or digital inputs, on which the sensors can be attached. The variety of environmental sensors is huge, from soil moisture and air temperature to soil PH and chlorophyll levels. Such applications require ultra dense networks consisting of thousands of nodes to report information about each plant's *micro-climate.*

The existing commercial WSN technologies utilize typical Marconi-type radio for wireless connectivity, such as ZigBee, Bluetooth, 802.11 and the like [1]. These radios are usually expensive and energy consuming, because they consist of complex *active* radio frequency (RF) components. Typically, such a radio consists of amplifiers, mixers, phase locked loops (PLLs) and

high quality filters. All these components increase the per node cost along with the energy demands, thus prohibiting the scalability of a WSN to dense network levels.

1.2 Scatter Radio

Instead of using *active* components radiating power to transmit information, a node may *reflect* induced RF signals to modulate data. The scatter radio principle was first presented in the 40s [2] and is based on the idea that a continuous wave, called carrier, is generated centrally and illuminates many nodes (RF tags). A tag's antenna is connected to an impedance switch that changes the antenna load according to the transmitted data. Different loads change the induced signal's phase or amplitude or both. That way, the signal is modulated and reflected back from the same antenna [3]. The scattered signals are then captured by a central receiver (reader) which demodulates and decodes each tag's information.

Although scatter radio is not a new idea, it has only recently been utilized for very specific applications. The most prominent commercial use of scatter radio is the radio frequency identification (RFID) systems. These systems use scatter radio to identify people, animals or products. Commercial standards have been developed for RFID [4], which are application specific and not flexible at all. However, this communication technology can really be useful to other scenarios, such as WSNs. In scatter radio, communication can be achieved by using a front-end consisting of a single radio frequency (RF) transistor, which minimizes both the energy requirements and the monetary costs of a sensor node. This allows large scale sensor deployment. Recent work has shown proof of concept, low-cost and low-power systems that can be used in dense scatter radio networks [5–8].

An overview of the scatter radio architecture used throughout this work is depicted in Fig. 1.1. A carrier emitter transmits a single tone continuous wave (CW) to illuminate the RF tag, which modulates and backscatters the data. A reader picks up the backscattered signals and decodes them to bits. As shown in Fig. 1.1, the system follows a *bistatic* architecture, meaning that the

carrier emitter and the reader are apart [9]. This is the main difference from the *monostatic* architecture, commonly used in commercial RFID systems, which incorporate the carrier emitter and the receiver in a single reader box.
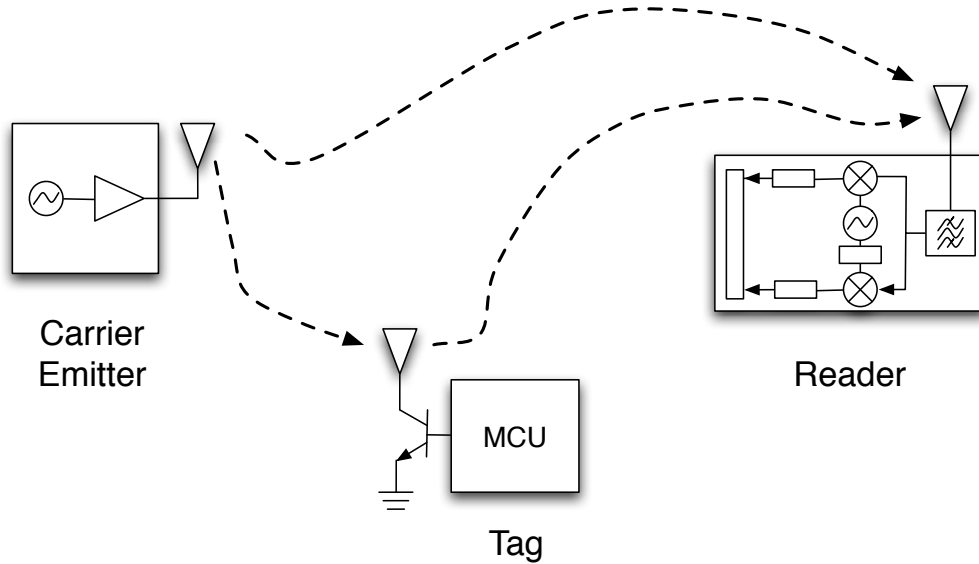
Figure 1.1: Bistatic scatter radio setup overview.

1.3 Bistatic Architecture

Extended field coverage is really important for agricultural networks. This means that the range for point-to-point links between the RF tags and the reader has to be maximized. However, the range of the link in typical RFID applications is really low. The range is inherently limited due to the following reasons:

1. Passive communication: Passive tags are used, which require energy harvesting to power their electronics. Commonly, these tags rectify a continuous wave (CW) signal, transmitted by the reader. Then the rectified energy is used to power-up the logic of the tags and backscatter the information. Thus, the achieved range is limited by the so-called "power-up" link [3].

2. High bitrate: Commercial RFID systems exploit high bitrates for tag-to-reader communication, on the order of hundreds of kbps. This means small bit duration, which results in reduced energy-per-bit and signal-to-noise ratio (SNR).

3. Monostatic architecture: The reader incorporates both the emitter that transmits the continuous wave needed for the scatter communication and the receiver that decodes the tag signals. It is easy to deduce that typical monostatic architecture suffers from round-trip path loss. The round-trip path loss is significant; the SNR at the receiver drops with the fourth power of reader-to-tag distance [9] or the eighth power of the distance for two-ray propagation model [10, 11]. This benefits the tags that lay closer to the reader, while the tags that are far can not be easily "picked up" by the reader.

Therefore, scatter radio has been redesigned to accommodate WSN applications. Three key points were made in [12, 13]:

1. Semi-passive tags (i.e. energy assisted) have to be utilized. These tags power their logic from batteries or low-cost renewable energy sources like low-voltage solar-panels [14].

2. Bitrate should be minimized to maximize energy-per-bit at the receiver. Although high bitrates are appealing, they are not a necessity for agricultural monitoring, because parameters like humidity, temperature or soil moisture change relatively slow. This allows longer tag sleep periods to conserve energy.

3. Bistatic architecture should be exploited to achieve long range scatter communication for WSN. By dislocating the carrier emitter from the receiver more flexible topologies can be set up. Carrier emitters can come in the form of an oscillator and a power amplifier only, making them really cheap. That way many emitters can be spread in a field maximizing the field coverage.

In this work, a prototype backscatter network is constructed. Particularly, by exploiting the bistatic architecture and utilizing a simple frequency division multiple access (FDMA) scheme multiple tags can communicate with the reader. Also, range extension is achieved by the use of channel coding on the tags.

Chapter 2

Bistatic Scatter Radio Link

As described in Chap. 1, the bistatic scatter radio system consists of a carrier emitter, a RF tag and a SDR receiver (Fig. 1.1) [8]. The carrier emitter illuminates the RF tag with a continuous waveform (CW), which is a single tone wave at the UHF band. The tag modulates the information using an RF transistor and scatters the modulated signal to the reader. In this chapter the signal model of the overall system is derived [15,16]. Both point-to-point and multiple access cases are discussed. Before presenting the models, some notation must be introduced. $x_i^l(t)$ represents the variable x of user l as a function of time, t. The i on the subscript may not be always present; when it is, it declares the bit, i.e. $i \in \{0,1\}$

2.1 Point to Point Signal Model

The equations and calculations that follow use the base-band equivalent model for simplicity.The flat-fading channels depicted in Fig. 2.1 are defined as:

$$h_{CR}(t) = a_{CR}\,\delta(t - \tau_{CR}) \tag{2.1}$$

$$h_{CT}(t) = a_{CT}\,\delta(t - \tau_{CT}) \tag{2.2}$$

$$h_{TR}(t) = a_{TR}\,\delta(t - \tau_{TR}) \tag{2.3}$$

with $a_* \in \mathbb{R}$. The corresponding phases introduced by the propagation delay are $\phi_{CR}, \phi_{CT}, \phi_{TR} \in [0, 2\pi)$, where:
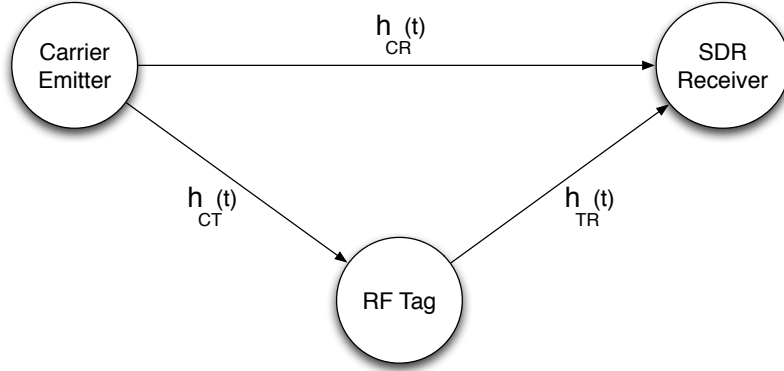
Figure 2.1: Bistatic channel model: the carrier emitter is dislocated from the receiving reader and the tag modulates the information on the CW.

$$\phi_{CR} = 2\pi\tau_{CR}, \tag{2.4}$$

$$\phi_{CT} = 2\pi\tau_{CT}, \tag{2.5}$$

$$\phi_{TR} = 2\pi\tau_{TR}, \tag{2.6}$$

The channels are *independent* and are considered constant in the duration of a *coherence* window. The signal transmitted by the carrier emitter is a continuous wave (CW) of frequency F_c and power $P_C = A^2/2$. Its base-band equivalent is given by the following equation:

$$c(t) = A\,e^{-j(2\pi\Delta f\,t+\Delta\phi)}, \tag{2.7}$$

where Δf and $\Delta\phi$ are the frequency and phase offsets between the carrier emitter and the SDR reader, respectively. $\Delta\phi$ is modeled as a random variable following uniform distribution in $[0, 2\pi)$ i.e. $\Delta\phi \sim \mathcal{U}[0, 2\pi)$. The RF tag receives the signal transmitted by the emitter, which has passed through the emitter-to-tag channel. The tag, in order to modulate the incident signal, switches between two antenna load reflection coefficients, Γ_0 and Γ_1. The antenna load reflection coefficient is given by the following equation:

$$\Gamma_i \triangleq \frac{Z_i - Z_a^*}{Z_i + Z_a}, \tag{2.8}$$

where Z_i corresponds to the tag load, $i \in \{0, 1\}$ and Z_a is the tag antenna impedance. The load reflection coefficient changes can be expressed as a function of time

$$\Gamma(t) \in \{\Gamma_0, \Gamma_1\}. \tag{2.9}$$

Recent work has exploited switching between M load values for high-order modulations [17, 18]. The tag complex base-band signal, as a function of time, is

$$x(t) \triangleq a_x(t)\, e^{j\phi_x(t)} = A_s - \Gamma(t), \tag{2.10}$$

where A_s is a load-independent antenna quantity called structural mode [19, 20]. In general, A_s is complex-valued and depends on the geometry and the materials used for the antenna construction. Also, Γ_i is complex-valued. Hence, the amplitude $a_x(t)$ is

$$a_x(t) \triangleq |\, A_s - \Gamma(t)\,| \tag{2.11}$$

and the phase $\phi_x(t)$ is

$$\phi_x(t) \triangleq \angle[A_s - \Gamma(t)], \tag{2.12}$$

i.e. it is the the angle of the complex quantity $A_s - \Gamma(t)$ in radians. More specifically, if $c(t)$ is the incident carrier waveform, the scattered waveform can be written as:

$$x_m(t) = s(t) \left(\left(A_s - \frac{\Gamma_0 + \Gamma_1}{2} \right) + \frac{\Gamma_0 - \Gamma_1}{2} u_i(t) \right) A_{CT} \, e^{-j\phi_{CT}} \, c(t)$$

$$= s(t) \left(v_0 + \frac{\Gamma_0 - \Gamma_1}{2} u_i(t) \right) A_{CT} \, e^{-j\phi_{CT}} c(t), \tag{2.13}$$

where $u_i(t)$ corresponds to modulation waveform of bit $i \in \{0, 1\}$ and differs between modulations. The v_0 term is a *DC* constant that depends on the antenna structural mode A_s and the load reflection coefficients Γ_0, Γ_1. The term $s(t)$ depends on the tag inherent scattering efficiency and tag antenna gain at a given direction. The tag efficiency is widely considered time-varying, due to the use of rectifiers on *passive* tags [3]. In our study, energy assisted (i.e. semi-passive) tags are used, hence $s(t)$ can be considered constant because no incoming rectification takes place. From now on, we consider this parameter constant and will simplify s(t) to s.

Thus, for a bit duration T, the received signal at the SDR reader is given by the superposition of the carrier emitter's continuous waveform and the backscattered tag signal passing through the channels $h_{CR}(t)$ and $h_{TR}(t)$, respectively:

$$y(t) = a_{CR} \, e^{-j\phi_{CR}} \, c(t) + a_{TR} \, e^{-j\phi_{TR}} \, x_m(t) + n(t)$$

$$= A \left(a_{CR} \, e^{-j\phi_{CR}} + a_{CT} \, a_{TR} \, e^{-j(\phi_{CT}+\phi_{TR})} s \left(v_0 + \frac{\Gamma_0 + \Gamma_1}{2} u_i(t) \right) \right) e^{-j(2\pi\Delta ft + \Delta\phi)}$$

$$+ n(t). \tag{2.14}$$

To simplify the notation the following abbreviations are used: $\phi_0 = \phi_{CR} + \Delta\phi$, $\phi_2 = \phi_{CT} + \phi_{TR} + \Delta\phi$ and $\phi_1 = \phi_2 + \angle(\Gamma_0 - \Gamma_1)$, as well as $m_0 = A \, a_{CR}, m_1 = A \, a_{CT} \, a_{TR} \, s \frac{|\Gamma_0 - \Gamma_1|}{2}$ and $m_2 = A \, a_{CT} \, a_{TR} \, s \, v_0$. Therefore, the received signal can be written as:

$$y(t) = \left(m_0 \, e^{-j\phi_0} + m_2 e^{-j\phi_2} + m_1 e^{-j\phi_1} u_i(t)\right) e^{-j2\pi\Delta Ft} + n(t), \ i \in \{0,1\}, \tag{2.15}$$

where $n(t)$ is a complex *Gaussian* random process, which stands for the thermal noise at the receiver. The carrier frequency offset (CFO) Δf can be estimated by using fast Fourier transform (FFT). The FFT calculates the signal's periodogram and then the offset of the DC term is estimated. The DC term contains tag-dependent parameters such as A_s, typically overlooked in the literature, which are really important for CFO estimation [20]. After CFO estimation and compensation, the reader must achieve bit-level synchronization. This is achieved by either energy or preambled-based correlation synchronization. Then, the received signal is sampled with sampling period T_s and the base-band signal samples for a bit duration T are given by:

$$y[k] \triangleq y(kT_s) = \underbrace{\left(m_0 e^{-j\phi_0} + m_2 e^{-j\phi_2}\right)}_{DC\,term} + m_1 e^{-j\phi_1} u_i(kT_s) + n[k], \ i \in \{0,1\}, \tag{2.16}$$

where $n[k] = n(kT_s) \sim \mathcal{CN}(0, 2\sigma_n^2)$ denoting the kth noise sample from random process $n(t)$. The low-pass power spectral density (PSD) of the complex *Gaussian* process $n(t)$ is given by:

$$S_{n,n}(F) = \begin{cases} \frac{N_0}{2}, & \text{if } \mid F \mid \leq W, \\ 0, & \text{elsewhere,} \end{cases} \tag{2.17}$$

where W is the base-band receiver bandwidth and each noise sample has power $\mathcal{E}\left[\mid n[k] \mid^2\right] = 2\sigma_n^2 = N_0 W$.

Since environmental sensing does not require high bitrate, low bitrate is utilized for power-consumption reduction. Given the extended bit duration,

it is assumed that the wireless channels between the carrier generator and either the reader or the tag, as well as between the tag and the reader, change within a *small* number of consecutive bits, i.e. the channel coherence time spans a limited number of bits. The same holds for the CFO, whose value has significantly changed within a limited number of bits [10].

It is important to define the following magnitudes to fully characterize the bistatic system. The instantaneous carrier-to-signal ratio (CSR) is defined as the instantaneous power ration between the transmitted carrier power and the reflected tag signal power and is given by the equation:

$$CSR(a_{CT}) \triangleq \frac{P_C}{P_T(a_{CT})}, \tag{2.18}$$

where $P_T(a_{CT})$ is the instantaneous tag reflected power that depends on the random amplitude a_{CT}. The average tag reflected power is given by:

$$P_T = \underset{a_{CT}}{\mathcal{E}} [P_T(a_{CT})]. \tag{2.19}$$

The average CSR is defined as the ratio of the average carrier power and the average tag power, i.e.

$$CSR \triangleq \frac{T_C}{P_T}. \tag{2.20}$$

The instantaneous received signal-to-noise ratio (SNR) per bit, in the reader, is defined as:

$$SNR_{inst}(a_{CT}, a_{TR}) \triangleq \frac{P_T(a_{CT}) \mid a_{TR} \mid^2}{2\sigma_n^2} L \tag{2.21}$$

and the average signal-to-noise ratio is:

$$SNR = \mathop{\mathcal{E}}_{a_{TR}, a_{CT}} [SNR_{inst}(a_{CT}, a_{TR})]. \tag{2.22}$$

2.1.1 Frequency Shift Keying Detection

The frequency shift keying (FSK) modulation utilizes a waveform of frequency F_i for each corresponding information symbol and requires as many basis functions as the transmitting symbols. To ensure orthogonality, the frequencies must have a certain spacing: $|F_i - F_j| = k\frac{1}{T}$, $k \, \epsilon \, \mathbb{N}$, $i \neq j$, where T is the bit duration. In scatter binary FSK (B-FSK) the tag switches between two distinct reflection coefficients, Γ_0, Γ_1, with two different frequencies F_i, $i \in \{0, 1\}$. Due to limited receiver bandwidth (See Chap. 3.3.3), $W \ll 3 \, F_i$, the waveform of frequency F_i, for each bit period T, can be written as:

$$u_i(t) = \frac{4}{\pi} \cos(2\pi F_i \, t + \Phi_i)\Pi_T(t), \; i \in \{0, 1\}, \tag{2.23}$$

where $\Pi_T(t)$ is the modulation pulse. In our case, a rectangular pulse of duration T is utilized, where T denotes the nominal bit duration:

$$\Pi_T(t) \triangleq \begin{cases} 1, & \text{if } 0 \leq t < T \\ 0, & \text{elsewhere} \end{cases} \tag{2.24}$$

Also, $\Phi_i \sim \mathcal{U}[0, 2\pi)$ models the phase mismatch between the tag and the reader when bit i is transmitted. It is assumed that Φ_0 and Φ_1 are *constant* and *independent* during a coherence window.

The samples of the received, digitalized signal of Eq.(2.17), with FSK modulation, are given by the following equation:

$$y[k] \triangleq y(kT_s) = \underbrace{\left(m_0 e^{-j\phi_0} + m_2 e^{-j\phi_2}\right)}_{DC\ terms} +$$

$$+ \frac{4}{\pi} m_1 e^{-j\phi_1} \cos(2\pi F_i k T_s + \Phi_i) \Pi_L[k] + n[k]. \qquad (2.25)$$

where $L \triangleq \frac{T}{T_s}$ is the receiver's oversampling factor and $\Pi_L[k]$ is the over-sampled version of the modulation pulse $\Pi_T(t)$.

The *DC* terms do not contribute any information, except from CFO estimation and can be eliminated by a DC-blocking filter. After the *DC*-blocking the digital waveform can be written as:

$$\hat{y}[k] = \frac{\hat{m}_1}{2} \left(e^{j(2\pi F_i k T_s + \Phi_i - \phi_1)} + e^{-j(2\pi F_i k T_s + \Phi_i + \phi_1)}\right) \Pi_L[k] + n[k], \qquad (2.26)$$

where $\hat{m}_1 = \frac{4}{\pi} m_1$ and $i \in \{0, 1\}$.

The scatter FSK modulation occurs directly at the pass-band, hence two subcarriers appear for each frequency F_i, at $\pm F_i$. More specifically, Eq.(2.26) shows that two complex basis functions exist for each frequency, hence two subcarriers exist for each frequency, one at the positive and one at the negative semiaxis, as shown in Fig.(2.2 -left). This makes the scatter FSK modulation completely different from the classic FSK modulation, which has one complex basis function for each frequency, as shown in Fig.(2.2 -right). This phenomenon implies that if the classic FSK receiver is utilized, then the system will have a 3 dB loss of information, due to the fact that it takes into account only two frequencies $+F_i$, $i \in \{0, 1\}$, while disregarding $-F_i$.
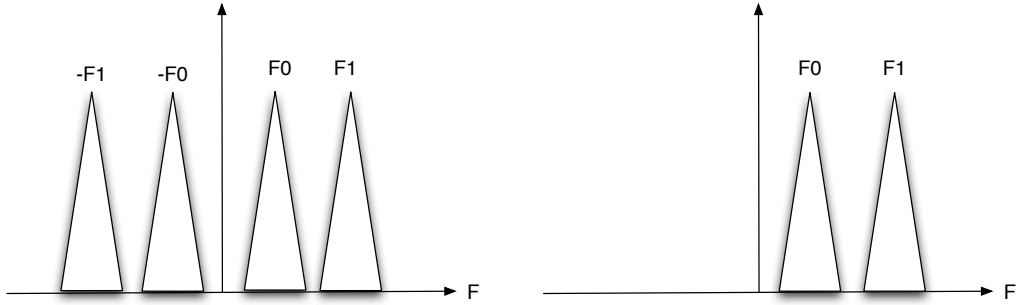
Figure 2.2: Complex base-band spectrum for scatter radio FSK (left) and 'classic' FSK (right). Two subcarriers per frequency exist in scatter radio FSK, in contrast to classic FSK.

For scatter B-FSK, a correlator must be utilized for each sub-frequency $\pm F_0$ and $\pm F_1$. Thus, four banks of correlators must exist as shown in Fig.(2.3).
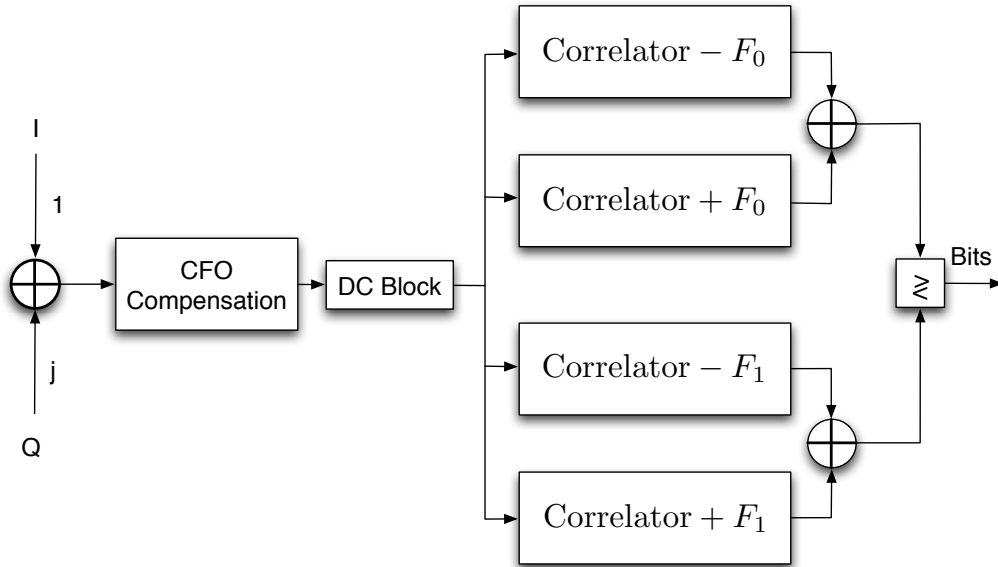
Figure 2.3: Scatter radio FSK basic signal processing chain.

For one bit duration T, each correlator processes $L = T/T_s$ samples the waveform and yields the statistics:

$$r_o^+ = \sum_{k=-\infty}^{+\infty} \hat{y}[k] \left(\Pi_L[k]\, e^{+j2\pi F_0 k T_s} \right)^* = \sum_{k=0}^{L-1} \hat{y}[k] e^{-j2\pi F_0 k T_s}$$

$$= \frac{\hat{m}_1}{2} \sum_{k=0}^{L-1} e^{+j[2\pi(F_0-F_i)kT_s+\Phi_i-\phi_1]} + n_0^+, \qquad (2.27)$$

where $n_0^+ = \sum_{k=0}^{L-1} n[k] e^{-j2\pi F_0 k T_s}$ is the sum of L independent complex *Gaussians*, $n_0^+ \sim CN(0, 2\sigma_n^2 L)$. Similarly, the outputs of the rest correlators are given by the following equations:

$$r_0^- = \frac{\hat{m}_1}{2} \sum_{k=0}^{L-1} e^{-j[2\pi(F_0-F_i)kT_s+\Phi_i-\phi_1]} + n_0^-,$$

$$r_1^+ = \frac{\hat{m}_1}{2} \sum_{k=0}^{L-1} e^{+j[2\pi(F_1-F_i)kT_s+\Phi_i-\phi_1]} + n_1^+,$$

$$r_1^- = \frac{\hat{m}_1}{2} \sum_{k=0}^{L-1} e^{-j[2\pi(F_1-F_i)kT_s+\Phi_i-\phi_1]} + n_1^-,$$

where $n_0^-, n_1^+, n_1^- \sim CN(0, 2\sigma_n^2 L)$. The random variables $n_0^+, n_0^-, n_1^+, n_1^-$ are statistically independent, since they are the projection of the low-pass Gaussian random process $n(t)$ on the orthogonal basis [21]:

$$\{e^{+j2\pi F_0 t}\Pi_T(t), e^{-j2\pi F_0 t}\Pi_T(t), e^{+j2\pi F_1 t}\Pi_T(t), e^{-j2\pi F_1 t}\Pi_T(t)\} \qquad (2.28)$$

When bit "1" is transmitted, the outputs of the correlators are:

$$r_0^+ = n_0^+, \qquad r_1^+ = \frac{\hat{m_1}L}{2}e^{-j\phi_1}e^{+\Phi_1} + n_1^+,$$

$$r_0^- = n_0^-, \qquad r_1^- = \frac{\hat{m_1}L}{2}e^{-j\phi_1}e^{+\Phi_1} + n_1^-.$$

On the contrary, when bit "0" is transmitted, the outputs of the correlators are:

$$r_0^+ = \frac{\hat{m_1}L}{2}e^{-j\phi_1}e^{+\Phi_1} + n_0^+, \qquad r_1^+ = n_1^+,$$

$$r_0^- = \frac{\hat{m_1}L}{2}e^{-j\phi_1}e^{+\Phi_1} + n_0^-, \qquad r_1^- = n_1^-.$$

Exploiting the statistics at the outputs of the correlators, we make use of the detector [15, 22]

$$z_1 \triangleq \mid r_1^+ \mid^2 + \mid r_1^- \mid^2 \overset{H_1}{\underset{}{\gtrless}} \mid r_0^+ \mid^2 + \mid r_0^- \mid^2 \triangleq z_0 \qquad (2.29)$$

2.2 Multiple Access Signal Model

In order to have multiple tags communicating simultaneously, frequency division multiple access (FDMA) is utilized. The network architecture and multiplexing protocol are discussed at length in Chap. 4. In this section the multiple access signal model is presented.

Since FDMA is utilized the multiple access link can be converted to multiple point-to-point links, utilizing different sub-carrier frequencies for each user. Since the users use different frequencies for their B-FSK modulation and guard bands are utilized, no interference or aliasing exists. In Fig. 2.4 the case of l-users communicating with the reader is presented and the analysis of the l-user signal model follows.

Again, assuming flat-fading channels, the tag signals pass through the channels h_{CT}^l and h_{TR}^l where l denotes the lth user and the channels are
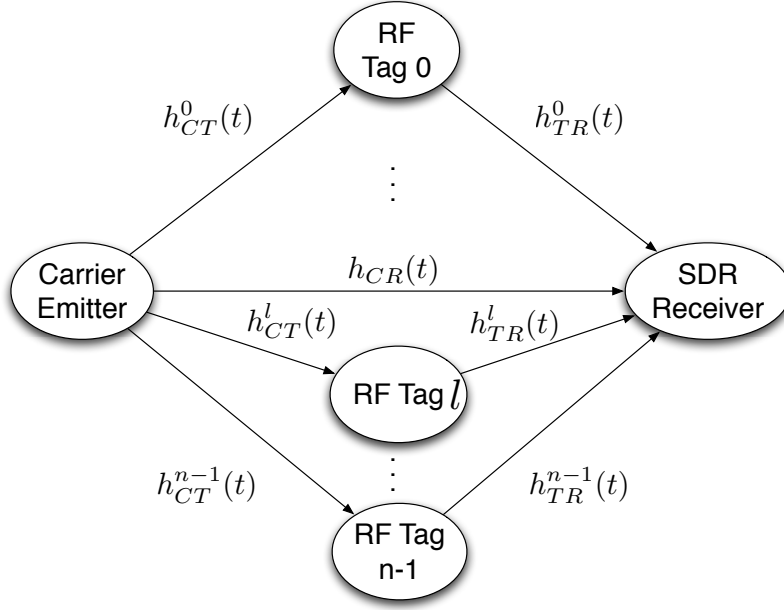
Figure 2.4: Multi-user bistatic channel model: n tags communicating with the reader.

given by Eq. 2.2 and Eq. 2.3, respectively. The resulting signals are the same as described in Eq. 2.15. The lth user's signal is given by the following equation:

$$y(t) = \left(m_0\, e^{-j\phi_0} + m_2^l e^{-j\phi_2^l} + m_1^l e^{-j\phi_1^l} u_i(t) \right) e^{-j2\pi\Delta F t} + n(t),$$

(2.30)

where $i \in \{0, 1\}$, $l \in \{0, ..., n-1\}$ and $n[k] = n(kT_s) \sim \mathcal{CN}(0, 2\sigma_n^2)$ denoting the kth noise sample for complex normal random process $n(t)$, which stands for the thermal noise at the receiver.

The reader receives the superposition of the carrier emitter continuous waveform and the backscattered signals of the n tags. After the down-conversion and the digitalization the samples of the received signal are given by the following equation:

$$y[k] = m_0 e^{-j\phi_0} + \sum_{l=0}^{n-1} \left(m_2^l e^{-j\phi_2^l} + \frac{4}{\pi} m_1^l e^{j(2\pi F_i^l kT_s + \Phi_i^l - \phi)} + e^{-j(2\pi F_i^l kT_s + \Phi_i^l + \phi)} \Pi_L[k] \right) +$$
$$+ n[k], \tag{2.31}$$

where F_i^l is the frequency of the subcarrier each user l uses for each bit and $m_1^l, \phi_i^l, m_2^l, \phi_2^l$ and Φ_i^l are the channel parameters for each user l.

The changes in the receiver and the detector are minimal. The CFO estimation and correction, as well as the *DC*-block filter are the same. For the synchronization and correlation a rake-like receiver is employed. The rake receiver has a finger for each user and each finger has four sub-fingers for each transmitted subcarrier. After the correlators, each user's signal is treated as a point-to-point link and the employed detector is derived in Eq. 2.29. The full receiver chain for n users is depicted in Fig. 2.5.
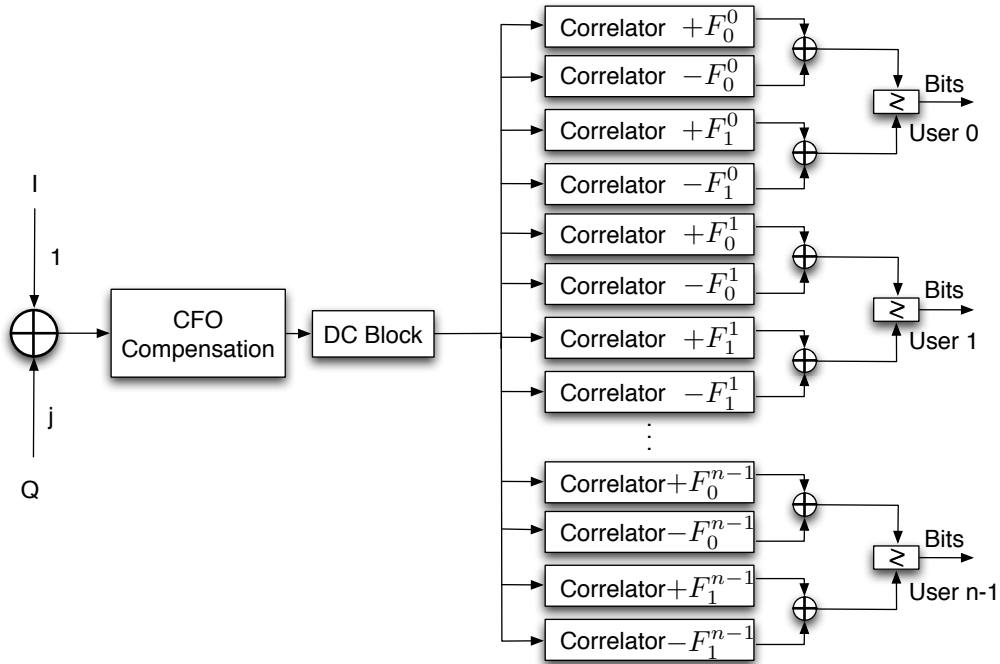
Figure 2.5: Scatter radio FSK, multiple users, basic signal processing chain.

Chapter 3

Scatter Radio Modules

3.1   Setup

The experimental setup used throughout this work is a newer version of the one presented in [22]. The setup consists of custom RF tags, a carrier emitter and a reader/receiver. The RF tags used for experimentation consist of an MCU, a SMA antenna connector and a single RF transistor. The tags are the main focus of this thesis and will be analyzed at length on Sec. 3.3. For carrier emitting, a WSN-like node with an embedded radio operating at the UHF band is utilized. The carrier's frequency and output power can be controlled via software. On the receiving end a commodity software defined radio (SDR) is used for capturing the backscattered signals at the UHF band (around 868 MHz), which is the European ISM band. The captured signals are processed in software on a host PC with modest processing capabilities and all signal processing is done on MATLAB environment with custom scripts. The setup is depicted in Fig. 3.1.
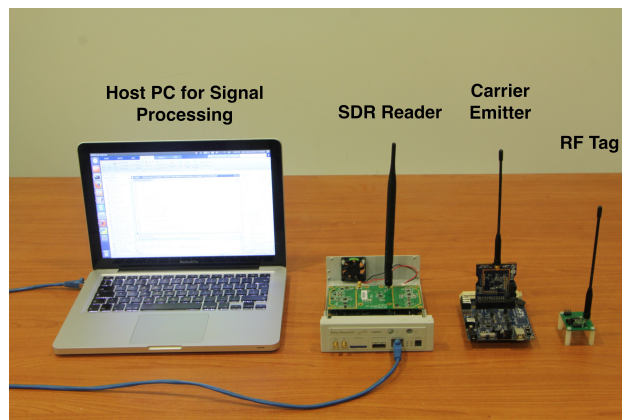
Figure 3.1: Bistatic scatter radio experimental setup.
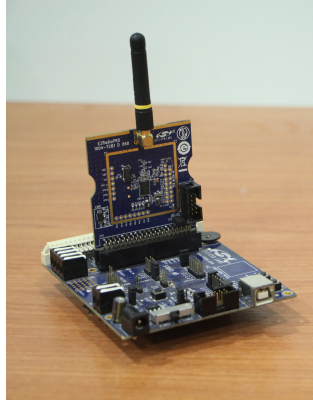
Figure 3.2: Carrier emitter evaluation board.

3.2 Carrier Emitter and Reader

For carrier generation and transmission a low-cost monolithic clip is used, containing an MCU and an embedded radio. The MCU is a 8051 architecture unit, which controls the radio via software and it is used to tune several radio parameters, such as carrier frequency, output power, etc. The carrier emitter is essentially a WSN node without any sensors or other peripherals attached and is used only for the transmission of the carrier signal. The embedded radio operates in the European ISM band $(866-868$ MHz$)$ and has a maximum power output of $+13$ dBm (approximately 20 mW). It must be noted that this node is low-cost and has the capability of battery operation, which makes it ideal for using multiple carrier emitters across a field to create cells extending communication range and field coverage (see Chap.4.2). The evaluation board of the carrier emitter is shown in Fig. 3.2.

The reader is responsible for the reception and processing of all backscattered signals. It consists of a receiver tuned in the UHF band to capture the backscattered signals and a series of processing blocks for tag decoding. In this work a software defined radio (SDR) was utilized, consisting of a UHF RF front-end (RFX900 daughterboard) and fast I/Q analog-to-digital converters (ADCs). The raw ADC data are send, via Ethernet, to the host PC, on which all signal processing is done in MATLAB software, with custom scripts. This gives great flexibility as the user can control the modulation

scheme, data rate, data encoding, etc. The SDR reader can "pick up" up to 8 MHz bandwidth, which is more than enough for low-bitrate scatter radio applications. Specific processing blocks are described in Chap. 2. The SDR receiver as well as the host PC are shown in Fig. 3.3.
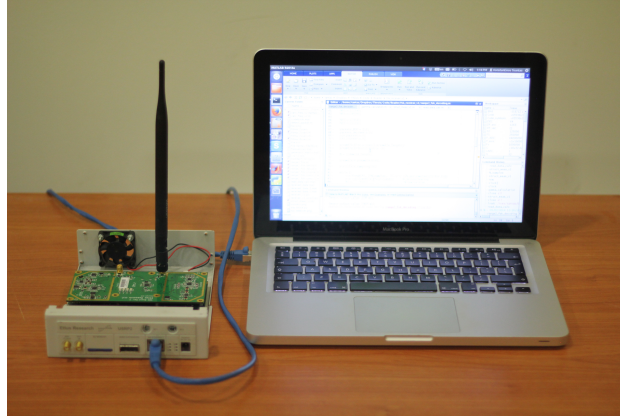
Figure 3.3: Software defined radio receiver and host PC.

3.3 Backscatter Tag

3.3.1 RF Tag Design

When constructing a wireless sensor network (WSN) for environmental sensing, high sensor node density is required. This results in the design of low-cost and low-power sensor nodes. Thus, the nodes should only consist of essential components. Since the scatter technology is utilized, the obvious choice would be the use of passive tags because of their low-cost and battery-less operation. But a semi-passive tag architecture is preferred as it increases the achievable up-link range (tag-to-reader communication), as shown in [3, 12].

In scatter radio, the modulation of the information is achieved by terminating the antenna between two loads; that way, the incident carrier waveform is reflected with altered phase and/or amplitude, according to the load that is selected each time. In practice, load switching is achieved by switching a single RF transistor. When the transistor is switched on, the antenna

is short-circuited and any incident wave is scattered back with π radians phase change. Respectively, when the transistor is switched off, the antenna is open-circuited and the incident wave is scattered back intact. This scheme is depicted in Fig. 3.4.
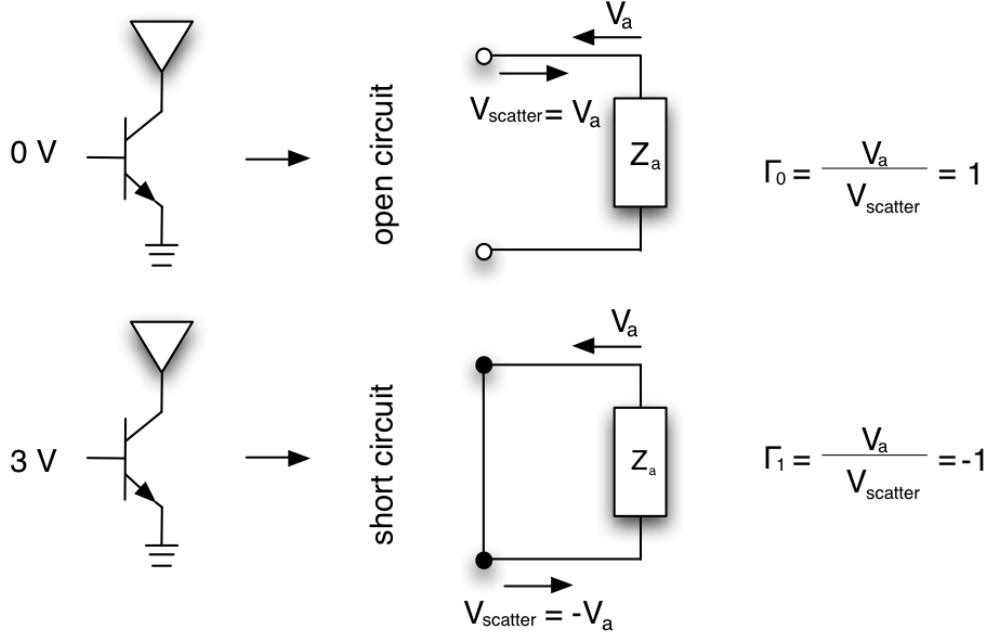
Figure 3.4: Scatter radio modulation with a RF transistor.

The first prototype developed consists of a low-power 8051 microcontroller unit (MCU) evaluation board from Silicon Laboratories and a custom front-end printed circuit board (PCB), which enables the scatter radio communication. The prototype is shown in Fig. 3.5. The MCU is a low-power 8051 architecture unit with C language program capability. Sensor inputs and LED outputs are available on the evaluation board. Also, it has two different powering modes. On dual-cell mode the MCU supports operation from $1.8V$ to $3.6V$ and on one-cell mode supports operation from $0.9V$ to $1.8V$. Hence, a $3V$ battery can be utilized for powering in both modes. The one-cell mode utilizes an integrated, high-efficiency, dc-dc boost converter to boost the voltage to the operating range. So, a small solar cell with an output voltage as low as $2V$ can also be utilized for powering, using the on-chip

dc-dc converter.
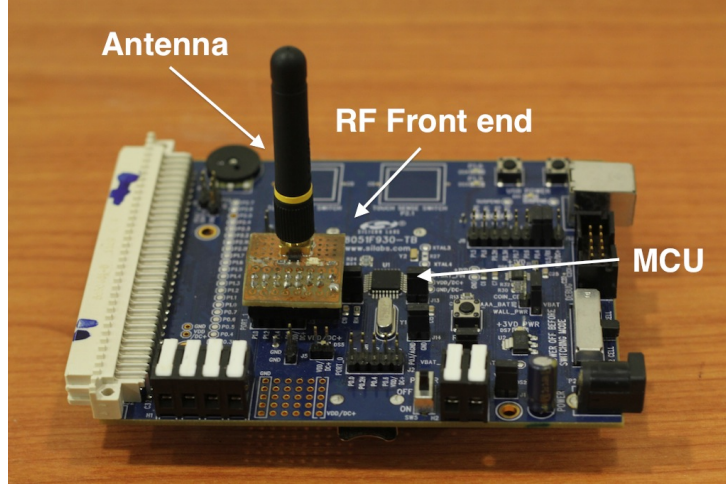
Figure 3.5: Semi-passive tag prototype.

The second prototype developed was a custom-made, one-layer PCB which combined, on the same board, all the components needed for the backscatter tag to operate. Everything i.e. the MCU, the programmer, the sensor inputs, the crystal oscillator, the RF transistor and the antenna connector are on the same PCB. Constructing a board with all the components on it, decreases the thermal noise of the whole circuit . In the first prototype the front-end and the MCU were on different boards and the ground plane was not common, thus increasing the total thermal noise of the circuit. Also, the front-end was changed by attaching a variable, voltage controlled load to the emitter of the RF transistor. This was used for experimentation with the antenna's structural mode. Two boards were constructed, one on the Telecom Lab's fabrication lab and one on a fabrication house outside the university. The two boards only differ in the construction method because the one built by the fab-house had silk-screen on, which made the soldering of the SMD components easier. The boards are depicted in Fig. 3.6.

The last prototype developed is also a custom made PCB, which is an upgrade of the aforementioned board. This prototype (Fig. 3.7) has a small form-factor, which can be waterproof-packaged and easily attached to plants, along with several types of sensors. This tag has ten input/output pins on
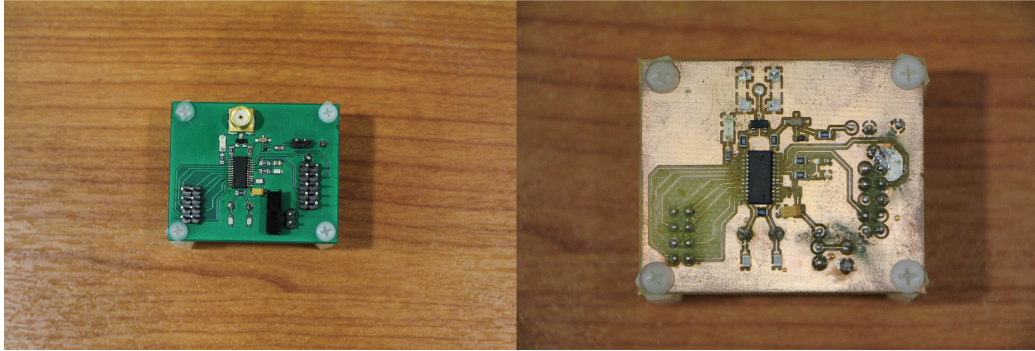
Figure 3.6: Second RF tag prototypes, where all the components are on the same board.

which sensors can be attached. The ADC can read each sensor's value and transmit with the appropriate packet information (See Chap. 4.3). Also the design is two-layered, thus resulting in smaller size and better electromagnetic (EM) shielding because both top and bottom layers are grounded and connected. The cost of these tags is almost 6 € without the SMA connector. The schematic and the bill of materials (BoM) of the tag can be found in the appendix (Chap. 7).

The last two prototypes are newer versions of the tag built in [22] with a lower power dissipation. The tag's schematics and layouts are given in the Appendix.
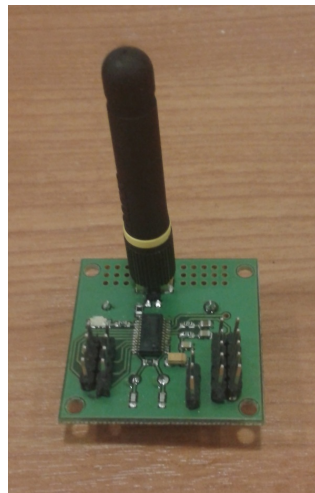
Figure 3.7: Final tag prototype with small form-factor.

3.3.2 Modulation: B-FSK frequency generation

For the bistatic scatter radio link, FSK modulation shows advantages over other modulations. This modulation provides us with extended range, simple multiple access and increased receiver sensitivity, which makes it ideal for scatter radio networks. In Fig.3.8 an instance of the B-FSK spectrum is depicted.
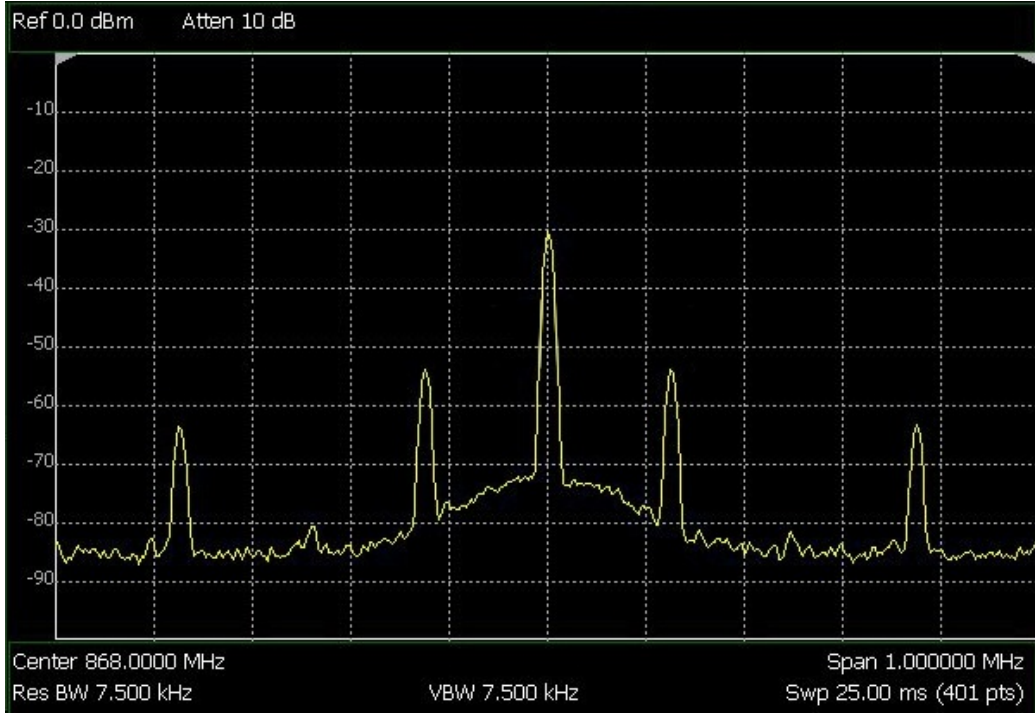
Figure 3.8: Pass-band B-FSK backscattered spectrum.

In B-FSK, the backscatter tag, switches between two distinct reflection coefficients Γ_0, Γ_1, with two different frequencies F_i for the corresponding bits $i = 0, 1$. To ensure orthogonality, the two frequencies (or subcarriers) must have a certain spacing: $|F_0 - F_1| = k\frac{1}{T}$, $k \in \mathbb{N}$, where T is the bit duration.

The rate of the switching is controlled by the MCU by toggling the pin connected to the transistor. This scheme generates a square pulse waveform of frequency F_i, which switches the transistor between the "on" and "off" state, that is two different reflection coefficient values. This results in the appearance of a square pulse waveform on the antenna. When the carrier

signal of base frequency F_c illuminates the tag, it is multiplied with the square pulse waveform. This multiplication creates the subcarrier signals on frequencies $F_c + F_i$ and $F_c - F_i$, which are the sub-carriers.

The MCU is responsible for generating the correct square pulse waveform which drives the transistor. The waveform must have the following characteristics:

- Precise frequency, which defines the subcarrier frequency.

- High enough amplitude to drive the transistor.

- Specific duration, which defines the data rate.

The frequency of the waveform, defines the subcarrier frequency. Thus, it is important that the generated waveform has precise frequency, in order to minimize the Frequency Offset. The frequency offset is an important problem which results in wrong correlation and detection. If the generation method is stable, the typical frequency offset should be the offset of the clocking circuit of the MCU.

The duration of the waveform is an other important parameter. The duration defines the data rate and hence, the bandwidth of the subcarrier. The duration must be precise otherwise the receiver can not operate at all.

The amplitude of the waveform is the last important parameter. The waveform's voltage changes the reflection coefficient of the antenna. The waveform has two values 0 V and V_{op}, where V_{op} is the operation voltage of the MCU. The MCU operates between $1.8 - 3.3$ V on dual-cell mode or $0.9 - 1.8$ V in one-cell mode. The switching transistor's base needs to be driven by a high enough voltage which will cause a state change. Since we are using a transistor that operates above 1.5 V, the dual-cell mode is preferred, because even if the battery's life is running out, the voltage levels are always high enough to drive the transistor. In one-cell mode, as the tag runs out of power, the voltage levels drop and approach 0.9 V and the MCU can no longer drive the transistor. In a later design, a different transistor can be used, such as BF1118 which operates in lower voltage, thus enabling us to use the less power-consuming one-cell mode.

The bibliography proposes many different ways to generate the waveform, such as voltage controlled oscillators (VCO), external synthesizers utilizing phase locked loop (PLL) and others. In our design, we utilized the MCU to do everything, from sensing and parsing the data to channel encoding and generating the communication subcarriers. The MCU has three ways to generate a square pulse waveform used for the modulation: a) Hardware timer b) Programmable counter Array (PCA) and c) Software generation.

The first two methods utilize a floating point adder and a hardware interrupt to operate. The main idea is that the user starts a counter at a specific value and every time the counter overflows a hardware interrupt is generated. Then in the interrupt service routine (ISR), the MCU toggles the control pin, thus creating a square pulse waveform. Hence, the period is controlled by the value of the reload value of the counter. The main limitation is that the counter uses a floating point adder. Floating point numbers are ideal for representing very small numbers with great accuracy. In order to generate high frequency signals, we need to enter a large overflow value, thus obligating the counter to overflow faster. But as the reload value increases, the ability of the adder to represent those numbers, decreases. Hence, the higher the output frequency, the lower the adder's precision. After testing both methods, is was observed that at 135 kHz output frequency, the error was almost 1 kHz, while at 260 kHz it was almost 5 kHz! This phenomenon makes these two methods unreliable.

The method that was used is the software generation method. It is based on the assumption that it is known how many clock cycles are needed for each instruction to be executed in the MCU's pipeline. The basic idea is that the control pin is toggled in the MCU's system clock frequency and then known delay is introduced to create a frequency divider. The instruction used to introduce the delay is the NOP instruction, which only requires one clock cycle in the pipeline. Hence, by combining many NOP instructions, we introduce the desired delay. The delay creates the period of the waveform, as the control pin stays at a given level for the a desired amount of time. As soon as the desired delay finishes, the pin is toggled, changing the voltage level, thus generating half a period of the desired waveform. A full period

includes two delay periods and two toggles of the control pin. In order to create the desired periodic waveform, we create a loop of delay and pin toggle. It is really important to note that each loop generates only half of the period of the waveform, so two loops are needed to create a full period.

This method has a major drawback which is the unknown delay introduced by the rest instructions the MCU has to perform on each loop. On each loop the MCU must increase the loop counter, evaluate the if-statement and then a jump must occur on another program counter, if needed. All these instructions introduce the unknown delay c. This delay can be quantified and is strongly correlated with the data rate, as shown later. A full period of the generated square pulse waveform is shown in Fig. 3.9.
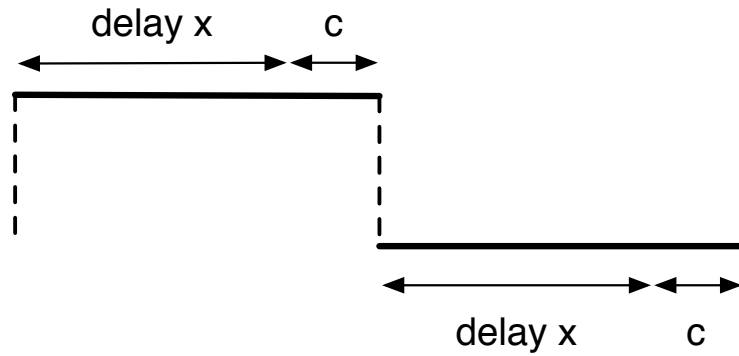

Figure 3.9: Frequency generation. Each period is created by introducing known delay x and unknown delay c.

The frequency of the signal generated by the frequency divider is given by the following equation:

$$F_{out} = \frac{\text{SYSCLK}}{(x + c)} \tag{3.1}$$

where SYSCLK is the system clock of the MCU and x, c are the known and unknown introduced delays in clock cycles.

The data rate (or bit period) in FSK depends on the duration the subcarrier exists on the air. Hence, it depends on the ending value of the for-loop, that recursively creates the subcarrier. This number is the number of periods that are needed, in order to create a specific bit period and is given by the following equation:

$$\frac{y}{2F_i} = \frac{1}{T_s} \Rightarrow y = \frac{2F_i}{T_s} \tag{3.2}$$

where x is the end-loop value, T_s is the symbol (or in our case bit) period and F_i is the corresponding bit frequency $i = 0, 1$. The number 2 in the equation exists because we need two loops to generate one period of the square pulse waveform.

For example, if we use $F_i = 125$ kHz and bit period $T_s = 1$ msec, then the number of half- periods the signal needs to consist of, is $y = 250$. And if we use $F_i = 200$ kHz and bit period $T_s = 1$ msec, then the number of half-periods the signal needs to consist of, is $y = 400$.

But since a 8-bit MCU is used the maximum value of a variable is 255. The MCU, in order to represent bigger numbers (e.g. the integer representation), uses two or more registers or memory slots to save them in. This creates a big problem since the for-loop instruction is a macro of many other instructions. On each loop, except from the nested code, the loop counter is increased, the if-statement is evaluated and then a jump occurs to a different program counter, if needed. If the value of the statement variable exceeds 255, then the MCU changes all the internal execution instructions for the add, save and brunch evaluation instructions. This results in bigger execution times for each instruction in the MCU's pipeline, hence the c parameter changes. This change forces us to change the known delay x on each period

in order to compensate for the change of c.

This is the huge trade-off of this method. The data rate affects the creation of the subcarrier frequency in a way that is not easily predicted. Extensive testing showed that as the end-loop value increases, the unknown delay c increases more than once. The function by which it changes is shown below in fig. 3.10.

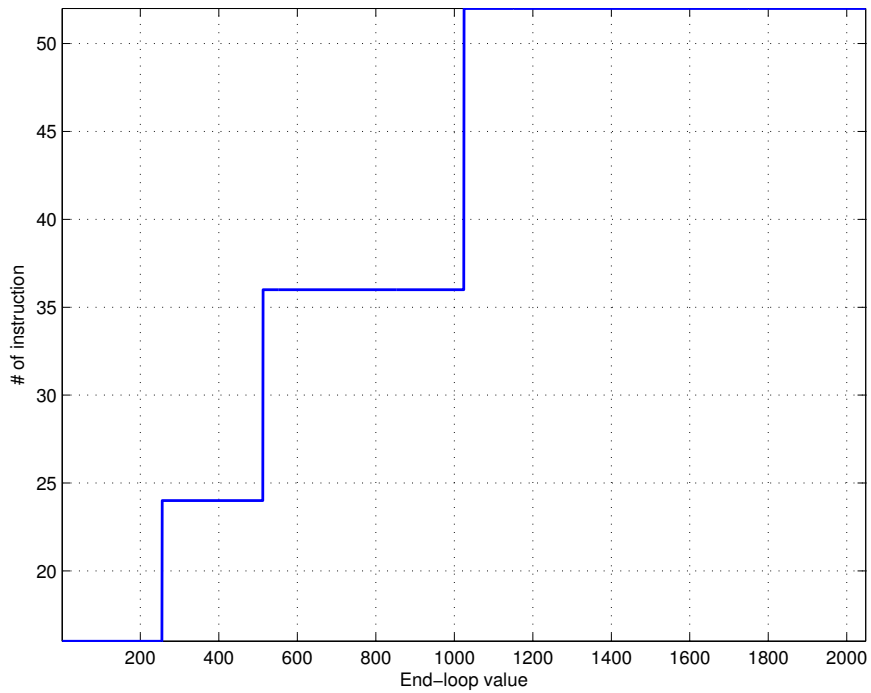Figure 3.10: Number of delay instructions introduces by the MCU vs. the end-loop variable value.

Because of this problem, different library files were created in order to have specific subcarrier frequencies at specific data rates.

3.3.3 Frequency Generation Limitations

Number of Available Frequencies The FSK modulation uses a subcarrier F_i for each corresponding bit $i = 0, 1$. Hence, each node must have two

basic subcarrier frequencies on which it communicates with the base station. But the big question is "How many pairs of subcarriers can we create?" using the aforementioned software method.

The output of the frequency divider, created by the software method, is analogous to the system clock and inversely analogous to the total delay, as shown in equation 3.1. This function has the following characteristic: because of the big numerator, i.e. $25 \cdot 10^6$, as the denominator decreases, the output value increases rapidly. So, as the total delay decreases creating higher frequencies, the gap between the generated frequencies increases. Hence, the MCU can create a huge amount of low frequency signals but, as the frequency gets higher, the number of generated signals decreases.

Another big question is "How many of these frequencies are usable?". To answer this question we need to consider the communication and the networking aspect of the problem. The FSK modulation needs a specific spacing between the subcarriers in order to ensure orthogonality. This constraint must be relaxed because the generation of subcarriers, which satisfy the orthogonality criterion, is not always possible. So, two subcarriers are selected for each node with spacing more than $\frac{1}{2T}$ and, if possible, the following condition must hold: $F_1 = 2 \cdot F_0$. This condition ensures that the spacing is always $k \frac{1}{2T}, k \, \epsilon \, \mathbb{N}$ and also if the pairs are selected this way, the data rate is easier to control. This selection leads to the same end-loop values for both F_0 and F_1 but, when sending the F_1 frequency signal, two periods are sent instead of one.

Modulation and the 3rd harmonic problem   From basic communication theory it is known that for optimal modulation Nyquist pulses must be used. A signal $u : \mathbb{R} \to \mathbb{R}$ is called a Nyquist pulse, with parameter T, if for $l \, \epsilon \, \mathbb{Z}$,

$$u(lT) = \begin{cases} 1, & \text{if } l = 0 \\ 0, & \text{if } l \neq 0 \end{cases} \qquad (3.3)$$

The use of Nyquist pulses on both the transmitter and the receiver si-

multaneously maximizes the signal to noise ratio (SNR) and minimizes the inter-symbol interference (ISI). In our modulation scheme square pulses are used to modulate the information. These pulses are, marginally, Nyquist pulses and thus they satisfy the Nyquist criterion. But because the classic 2-FSK is used, the phase change of the signal from each sent bit to the next, occurs on the bit boundary. This discontinuity of phase results in the appearance of the signal's odd harmonics (See Fig. 3.11). The even harmonics are all eliminated by constantly keeping the signal's duty cycle at 50%.
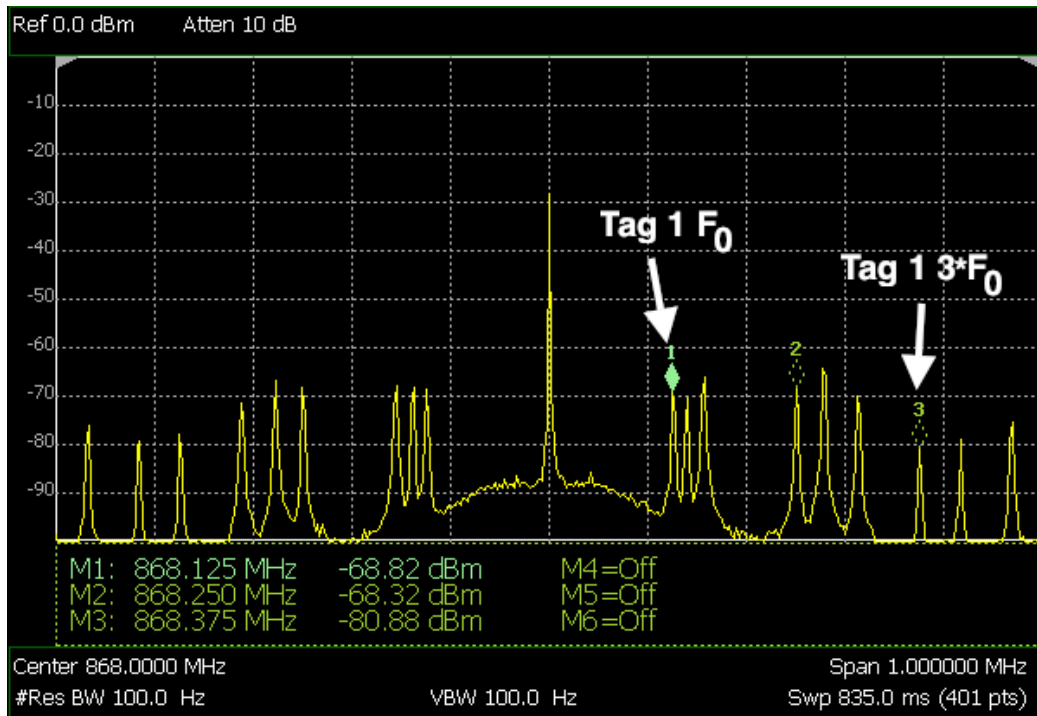
Figure 3.11: Spectrum of three scatter tags. Each tag communicates on different frequencies. The 3rd harmonic prohibits us from using frequencies above $3F_0$

The third order harmonics are a huge tradeoff of this modulation method. If they are not eliminated, the available communication bandwidth shrinks. It easy to deduce that if the first generated frequency is at F_0, then the available communication bandwidth is $BW = 3F_0 - F_0 = 2F_0$. This happens because at $3F_0$ and above, the third order harmonics exist. Because the frequency of all the signals are aliquots of the system clock, there may exist

frequencies higher than $3F_0$ that are usable but this is not flexible at all (See Fig. 3.12). Ways to overcome this problem are proposed in chap. 6.2.
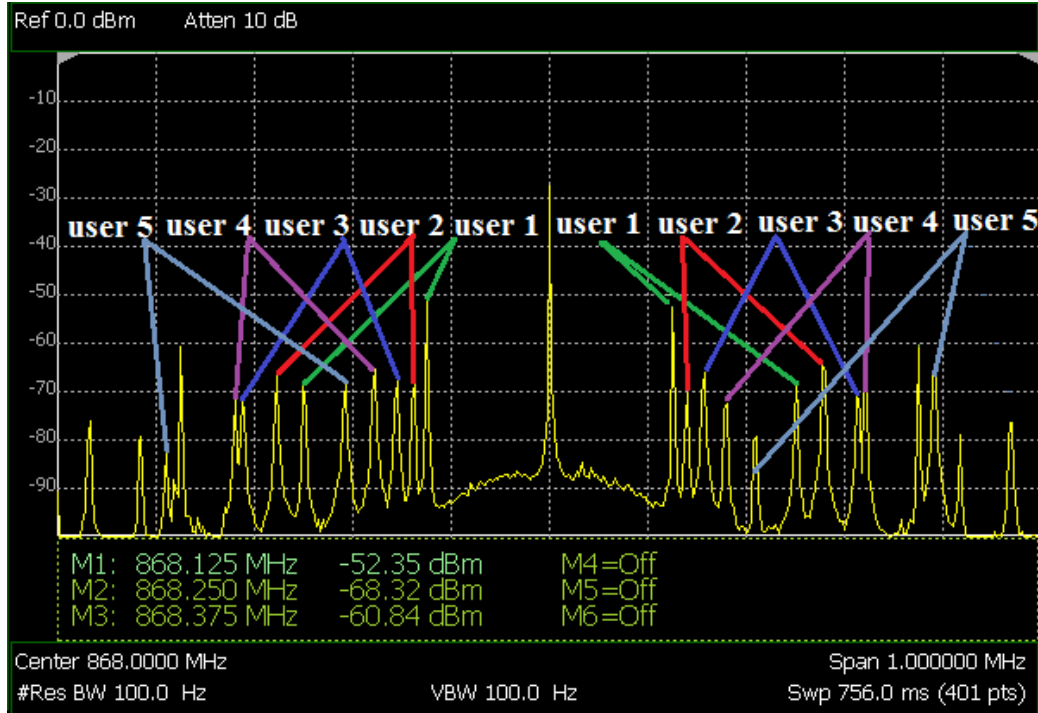
Figure 3.12: Spectrum of five scatter tags. The 3rd harmonic of tag 1 F_0 is too close to tag 5 F_1. The third harmonic and the base frequency could overlap, resulting in interference.

Chapter 4

Constructing a network

4.1 Network Model - FDMA - Topology

This work focuses on the creation of a network utilizing the bistatic architecture and consisting of the aforementioned components: tags/nodes, multiple carrier emitters and a centralized reader. Typical wireless sensor network architectures consist of the sensor nodes communicating with each other and a sync node collecting the data. The communication and multiplexing protocols developed for such networks are numerous (e.g. statistical multiplexing, time division multiple access (TDMA)) but all protocols require node-to-node or sync-to-node communication.

Before discussing the protocol, the network's architecture must be determined. In monostatic scatter architectures the reader is both the emitter and the receiver. This means that in order to have complete coverage of a space, either many readers must be employed or many antennas must be used on the reader or both. This makes these architectures really expensive. In the bistatic architecture the emitter is dislocated from the reader. This allows the placement of the emitters either randomly or on strategic positions around a field with several tags. This scheme increases the likelihood of a tag to be close to an emitter, thus increasing the overall field coverage, as more emitters are placed around. This leads to the creation of a "cell" around each emitter. Only one reader/sync, with enough computational power, can be used for processing multiple tags simultaneously. The reader is only responsible for capturing the superposition of the transmitted signals and decode the information. Thus, a SDR with only signal processing blocks can be used. A prototype network topology is depicted in Fig. 4.1.

In WSNs several multiplexing protocols have been developed over the
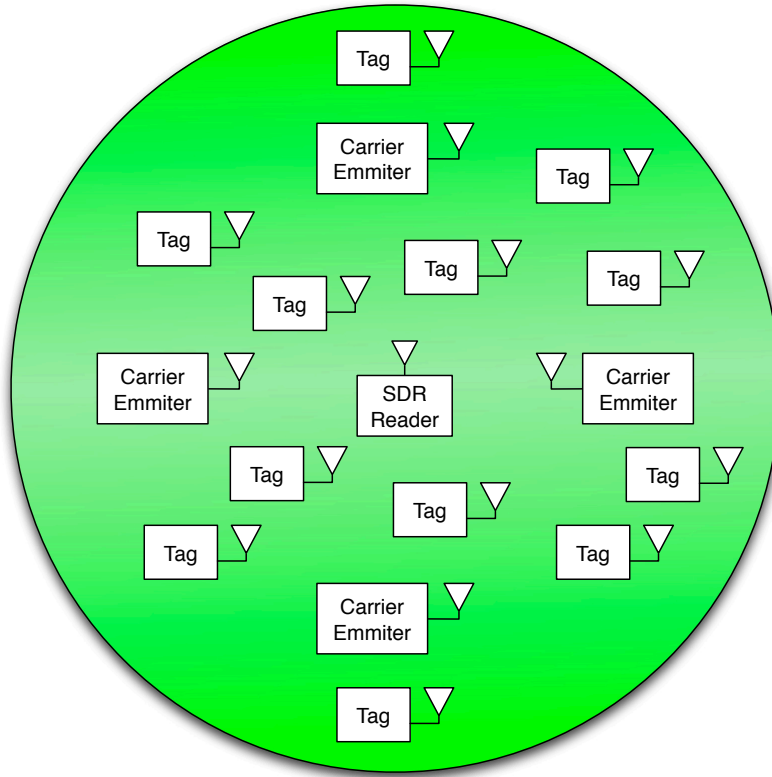
Figure 4.1: Possible network topology, with multiple tags and carrier emitters and a RF reader in the center.

years. But most of them require the existence of the down-link (sync-to-node communication). In our case the down-link does not exist, since the tags are receiver-less. Hence, the only multiple access scheme that can be utilized is frequency division multiple access (FDMA). This scheme is commonly used in analog and digital television and also the combination of FDMA and TDMA is used in worldwide cellular communications. In FDMA the communication medium, in our case free space, is divided in a number of channels, one for each user, the scheme is depicted in Fig. 4.2. B-FSK is ideal for frequency division multiplexing (FDM) since each user is given a different pair of frequencies to communicate on.

The implementation of the FDMA scheme is not trivial as many problems need to be solved. The first problem that has to be addressed is the
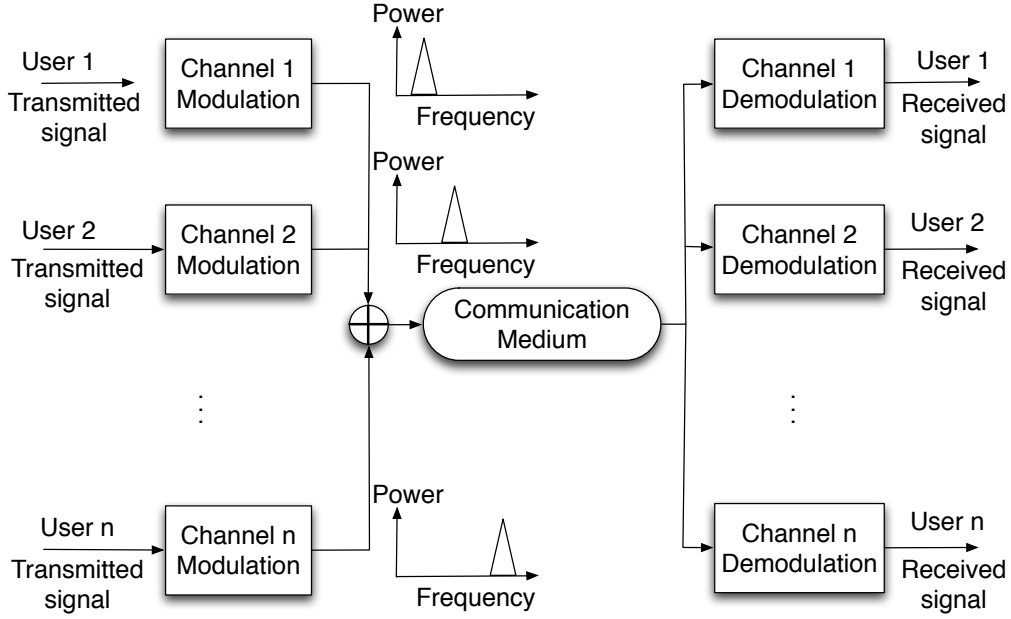
Figure 4.2: Frequency division multiple access scheme. Each user transmits on a different frequency channel, thus no interference to the other users exists.

communication bandwidth. Since non-coherent B-FSK is used, each user's signal requires bandwidth $W = \frac{1}{T}$, where T is the bit period. The communication rate determines the bandwidth each user needs and ultimately the total number of users that can communicate simultaneously. In Sec. 3.3.3 we discussed the bandwidth limitations of classic non-coherent B-FSK. Since the 3rd harmonic of the first frequency exists, the available bandwidth is shrinked to only $3F_0 - F_0 = 2F_0$. Thus, F_0 must be carefully chosen. If F_0 is too close to the carrier there is a possibility that the signal utilizing F_0 will be "buried" by the carrier emitter's clatter. On the other hand, if F_0 is too far, the receiver's bandwidth will be too large. This way the receiver absorbs more noise which results in an increased noise floor (See Chap. 4.4), which decreases the receiver's performance. These trade-offs are really important. In this work, F_0 is set at 100 kHz, thus the available bandwidth is $W = 200$ kHz.

Apart from the available bandwidth, another important aspect of the network that must be addressed is the guard bands. Each user uses a pair

of frequencies and each transmitted signal uses W bandwidth. But it is not possible to create all frequencies that are apart from each other by W because of the utilized frequency generation scheme. Even if it were possible, it is bad practice not to leave some space between the users because even the slightest frequency offset at the tag would result to interference. Thus, guard bands must be introduced around each available communication frequency (See Fig. 4.3). But the guard band depends on the communication rate. In this work the communication rate is 1 kbps, hence each signal's bandwidth is $W = 1$ kHz. The guard band is set at 500 Hz from either side of the signal, summing to a total 1 kHz guard band. Therefore, each user need 3 kHz bandwidth, two for each frequency.
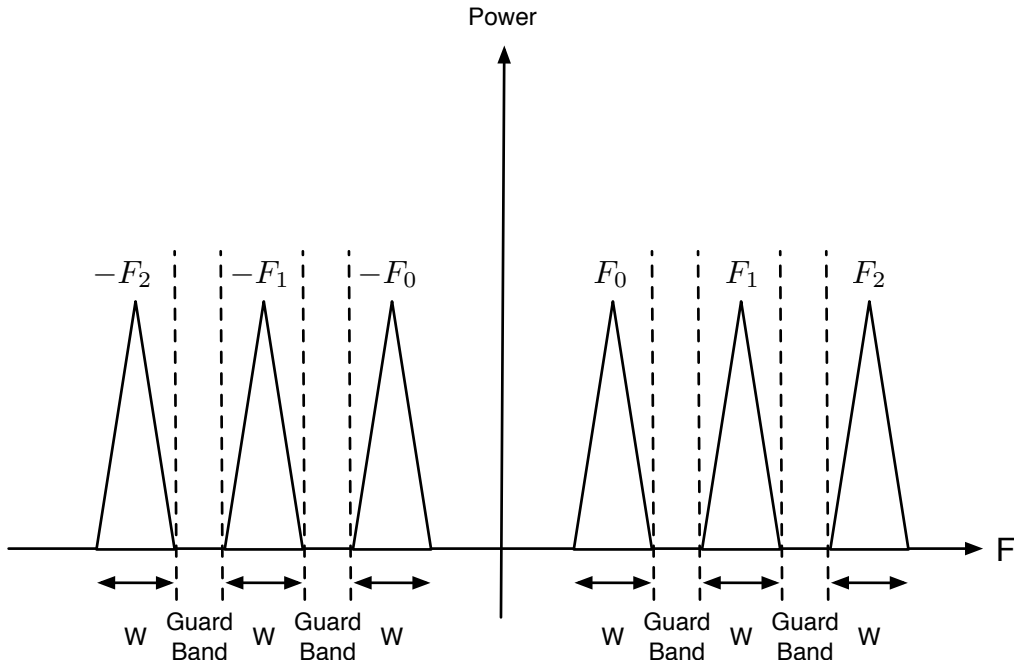
Figure 4.3: Schematic of the spectrum of the FDMA scheme using guard bands.

Theoretically, the aforementioned problems shrink the total number of users/ tags that can communicate simultaneously to only 66. But not all communication frequencies are available. Hence, the total number of users is around 50. In Fig. 4.4 the spectrum at the receiver of five communicating

tags is shown.
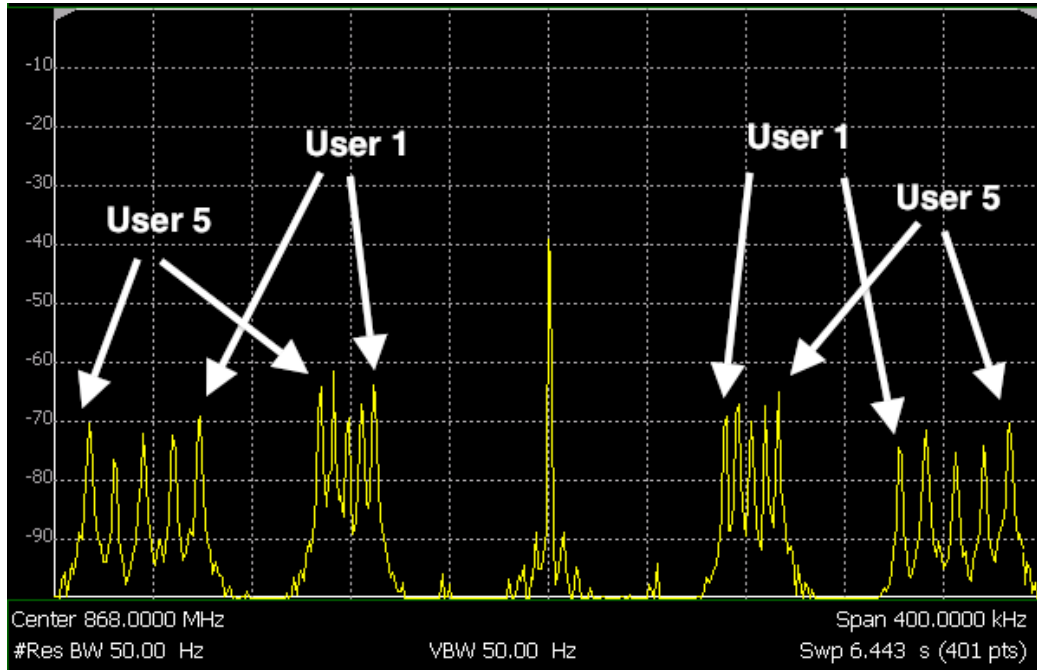
Figure 4.4: Pass-band FSK spectrum of five tags utilizing FDMA.

4.2   Cells and Carrier Emitters

The network architecture allows us to create communication cells. Each cell consists of an emitter and an arbitrary number of tags, as shown in Fig. 4.5. The emitter's radiation field is not circular and changes according to the environment. Hence, cells will intersect with each other and thus neighboring cells can not contain tags communicating on the same subcarrier frequencies. The same subcarriers can be used on not-neighboring cells that utilize TDMA. The carrier emitters used in this work employ an embedded radio, working at 900 MHz. The emitters can communicate with each other and with the reader who can assign time slots to each emitter. If non-intersecting carrier emitters use different time slots to emit their carrier waveform, then the tags can use the same subcarriers, since two tags with using the same frequencies will never transmit simultaneously. Hence no collision shall occur at the reader, thus, increasing the total network's capacity. Also, if the emitter TDMA scheme is employed, then directional antennas can be utilized at the reader. The reader will know which cell is supposed to transmit and will use the appropriate antenna port to receive (more on Chap. 6.2).
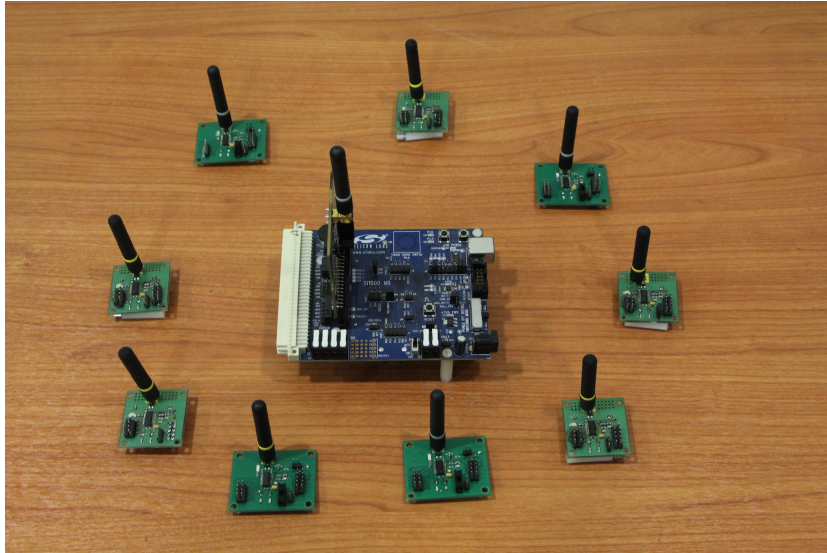
Figure 4.5: A simple cell example. Nine scatter tags and an emitter.

It is important to note that by placing many carrier emitters on the field,

the emitter-to-tag path loss can be statistically reduced, since it will be more likely for a tag to lay close to a carrier emitter. This extends the total field coverage without employing extra readers. The cell architecture is depicted in Fig. 4.6.
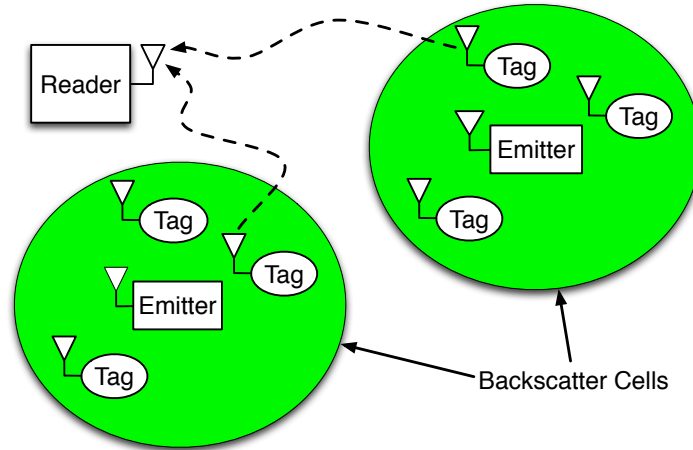
Figure 4.6: Scatter radio field with sensors/RF tags. Multiple carrier emitters are placed in the field to illuminate tags, along with a centralized receiver/reader.

4.3   Packet Format

Since FDMA is utilized each tag communicates on its own specific frequencies. When a tag wants to communicate with the reader, it sends a packet. The length of the packet varies but can not be large because of the small bitrate. If the packet is large then the channel parameters and the CFO may change during its transmission. The packet consists of five fields:

- Preamble (variable length, minimum 25 bits)

- ID (static length, 4 bits)

- Utility bits (static length, 3 bits)

- Coding scheme identifier (static length, 2 bits)

- Sensor ID (static length, 3 bits)

- Data (variable length, minimum 16 bits)

Preamble	Tag ID	Utility	Coding Scheme	Sensor ID	Data
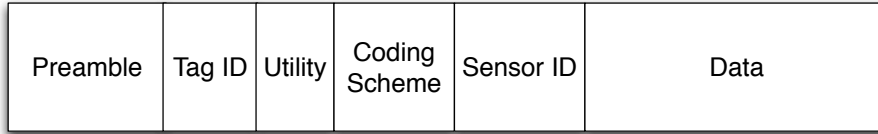
Figure 4.7: The packet format of the backscatter tag.

The preamble field is used for bit-level synchronization at the receiver. Its length is decided when the network is programmed and installed. After the synchronization and the detection, the reader checks and saves the tag's ID. The utility bits are used by the MCU to transmit any problems regarding the tag's operation which can be solved by the administrator of the network. Possible messages include tag's battery levels or sensor problems. Since more than one coding schemes are programmed on the tag's memory, a code-ID must exist in order for the reader to know which decoding algorithm to use. Also a sensor ID is utilized because the tag can support more than one sensors. Finally, the data section is a variable length field containing the coded data. Its length depends on the coding scheme employed and the minimum length is 16 bits and it is the uncoded information bits.

The aforementioned packet format gives flexibility to the system, making it more robust, as the reader can choose from a variety of decoding algorithms on-the-fly, while gathering information of each tag's condition without special packets sent by the tag. The received data (tag ID and infowords), along with the network's information can then be uploaded to a website allowing online network observation.

4.4 Near-Far Problem

The near-far problem is a situation that is common in wireless communication systems. It is a condition in which a receiver captures a strong signal and

thereby makes it impossible for the receiver to detect a weaker signal [23]. Hence, the receiver's sensitivity is compromised. Before studying the sensitivity problem, we need to define three important receiver parameters.

In many analog circuits, the signal-to-noise ratio (SNR) is defined as the ratio of the signal power to the total noise power. Most front-end receiver blocks are characterized in terms of their noise figure rather than the input-referred noise. The most commonly accepted definition of noise figure is:

$$NF = \frac{SNR_{in}}{SNR_{out}}, \tag{4.1}$$

where SNR_{in} and SNR_{out} are the signal-to-noise ratios measured at the input and output, respectively. It is important to understand that Eq.4.1 is a measure of how much SNR degrades as the signal passes through a system.

With the definition of the receiver's front-end noise figure, we can define the receiver's sensitivity as the minimum signal level that the system can detect with acceptable signal-to-noise ratio (SNR). To calculate the sensitivity, we write,

$$NF = \frac{SNR_{in}}{SNR_{out}}$$
$$= \frac{P_{sig}/P_{RS}}{SNR_{out}}, \tag{4.2}$$

where P_{sig} denotes the input signal power and P_{RS} the source resistance noise power, both per unit bandwidth. It follows that

$$P_{sig} = P_{RS} \cdot NF \cdot SNR_{out}. \tag{4.3}$$

Since the overall signal power is distributed across the channel bandwidth B the two sides of Eq.4.3 must be integrated over the bandwidth to obtain the total mean square power. Thus, for a flat channel,

$$P_{sig,tot} = P_{RS} \cdot NF \cdot SNR_{out} \cdot B. \tag{4.4}$$

Changing the notation slightly and expressing the quantities in dBm, we have

$$P_{in,min|dBm} = P_{RS}\,|_{dBm/Hz} + NF\,|_{dB} + SNR_{min}\,|_{dB} + 10\log B, \tag{4.5}$$

where $P_{in,min}$ is the minimum input level that achieves SNR_{min} and B is expressed in hertz. Equation 4.5 predicts the sensitivity as the minimum input signal that yields a given value for the output SNR. The sum of the first three terms is the total integrated noise of the system and is called "noise floor". This is a really important parameter because any signal under the ADC's noise floor can not be detected.

The last parameter we need to define is the receiver's dynamic range. The dynamic range is generally defined as the ratio of the maximum input level that the receiver's circuit can tolerate to the minimum input level at which the circuit provides a reasonable signal quality.

These parameters quantify the near-far problem. The dynamic range of one or more stages of the receiver can limit the receiver's ability to detect a weak signal in the presence of a strong signal, resulting in decreasing the receiver's sensitivity. The near-far problem, usually, refers to a specific case of this in which the ADC resolution limits the range of signals the receiver can detect. To solve this problem the receiver's automatic gain control (AGC) unit must reduce its gain to prevent ADC saturation, which causes the weaker signal to fall under the ADC's noise floor.

This phenomenon is a big issue of the backscatter networks. Consider a field with two tags and a reader. Tag B is placed far from the reader, while tag A is placed closer, as depicted in Fig. 4.8. The reader receives the superposition of the two signals. Assuming that the channel applies the same attenuation to both tags, the received signal strength (RSS) of Tag A

P_A, will be stronger than P_B because tag A is closer to the reader. This will blind the reader, resulting in false detection for tag B.
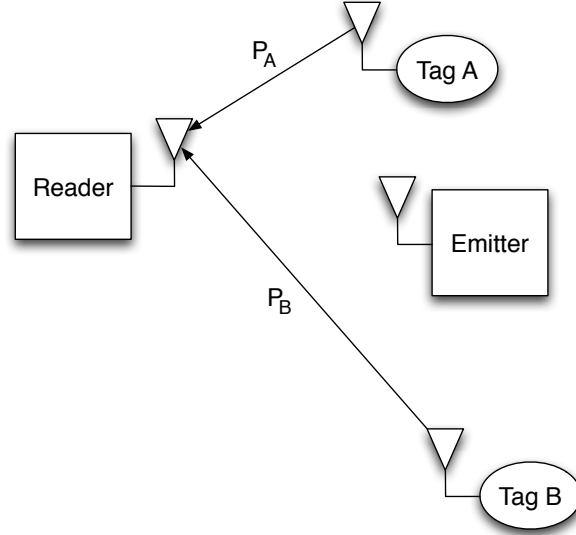
Figure 4.8: Near-far problem. Two tags, one closer to the reader than the other transmit to the reader. Tag A, the one closer to the reader, blinds the reader resulting in false detection of tag B.

Now consider a scenario where n tags, k emitters and one reader exist on the field (Fig. 4.9). The field is divided in cells (as described in Chap. 4.2). But the area that the adjacent cells cover will always intersect. Hence, a tag's signal will be transmitted to the receiver following more than one "strong" paths. If the phase of the tag's received signals at the reader align, then constructive addition of the signals occurs, resulting in higher RSS. If the tag is closer to the reader, so that the channel attenuation is smaller, tag's A received signal will blind the reader. This is why the near-far problem is extremely important in backscatter networks.

The solution of this problem is not trivial. Most telecommunication systems (e.g. CDMA, GSM, 3/4G) employ a wide range of schemes to counter the effects of the near-far problem. Some of these schemes include expensive high sensitivity ADCs on the receiver, dynamic output power control on the transmitters, which means nearby transmitters decrease their output power
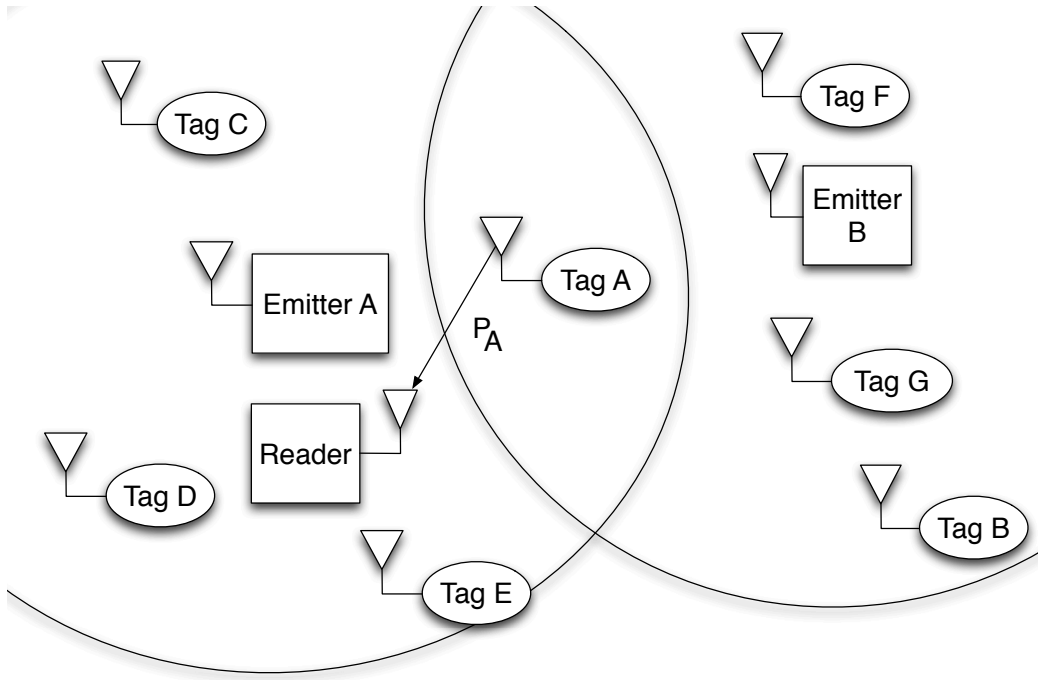
Figure 4.9: Near-far problem on multiple cells. Tag A belongs to two cells. If constructive addition occurs then the RSS blinds the reader, resulting in false detection of the tags farther away from the reader.

so that all signals arrive at the receiver with similar signal strengths or time division multiple access (TDMA), so that the transmitters do not transmit at the same time [10]. But in our case, most of these schemes can not be utilized, since we use a receiver-less tag, while reader-to-tag communication is required.

Chapter 5

Channel Coding - Linear Block Codes

5.1 Range Considerations

The most important limitation of commercial RFID systems is their small range. The use of passive tags limits the up-link range to only a few meters. In [13] the up-link range is extended with the use of semi-passive tags and the bistatic architecture. In this work, channel coding is employed to increase the range of the tag-to-reader link, by decreasing the probability of error for a given SNR. The main idea of channel coding is to exploit the redundancy introduced by the encoder in order to increase the reliability of reception, by sacrificing transmission rate. The tag utilizes a 8-bit MCU for the encoding process, which means that the computational power of the processor is limited. Thus, codes with low computational and memory requirements must be utilized. Linear block codes need only a simple matrix multiplication for the encoding process and this is the reason they were utilized in this work. This chapter introduces the basics of linear block codes encoding and decoding and also presents the tag's encoding schemes.

5.2 Encoding of Linear Block Codes

Consider a source that produces symbols from an alphabet $\mathcal{A}$ having q symbols, where $\mathcal{A}$ forms a field. We refer to a tuple $(c_0, c_1, \dots, c_{n-1}) \in \mathcal{A}$ with n elements as an n-vector. An (n, k) block code $\mathcal{C}$ over an alphabet of q symbols is defined as a set of q^k n-vectors called codewords or code vectors.

The objective of the encoding is to map a sequence of k information bits

produced by the source, to $n \geq k$ coded bits. The new sequence is used for error detection and correction.

For a block code to be used for error correction purposes, there should be a one-to-one function associating a message $\mathbf{m}$ to its codeword $\mathbf{c}$. The simplest one-to-one function is a linear function. Hence, the encoder is a linear function mapping a binary tuple of length k to a binary tuple of length n ($f : \mathbb{B}^k \to \mathbb{B}^n$). Therefore, a linear block code $\mathcal{C}$ over the field $\mathbb{B}$. i.e the set containing all the possible codewords, is a k dimensional subspace of $\mathbb{B}^n$. This means that exist totally $\mid \mathbb{B}^k \mid = 2^k$ binary codewords.

Since a linear block code $\mathcal{C}$ is a k-dimentional vector space, there exist $\mathbf{k}$ linearly independent vectors in $\mathbb{B}^n$ that form a basis for the code. If we designate the vectors as $\mathbf{g}_0, \mathbf{g}_1, \dots, \mathbf{g}_{k-1}$, then every codeword $\mathbf{c}$ in $\mathcal{C}$ can be represented as a linear combination of these vectors,

$$\mathbf{c} = m_0\mathbf{g}_0 + m_1\mathbf{g}_1 + \dots + m_{k-1}\mathbf{g}_{k-1}, \tag{5.1}$$

where $m_i \in \mathbb{F}_q$. It must be noted that, since binary codes are assumed, all arithmetic in Eq.(5.1) is done modulo 2. If we consider the $\mathbf{g}_i$ as row vectors and stacking up, we form the $k \times n$ matrix G,

$$\mathbf{G} = \begin{bmatrix} \mathbf{g}_0 \\ \mathbf{g}_1 \\ \vdots \\ \mathbf{g}_{k-1} \end{bmatrix} \tag{5.2}$$

Let

$$\mathbf{m} = [m_0 \ m_1 \ \cdots \ m_{k-1}]$$

be the vector containing the k information bits. Then, 5.1 can be written as,

$$\mathbf{c} = \mathbf{mG}, \tag{5.3}$$

and every codeword $\mathbf{c} \in \mathcal{C}$ has such a representation for some vector $\mathbf{m}$. Since the rows of $\mathbf{G}$ generate the (n, k) linear code $\mathcal{C}$, the matrix $\mathbf{G}$ is called a *generator matrix* of $\mathbb{C}$. Representing the code thus requires storing only k vectors of length n, rather than the q^k vectors that would be required to store all codewords of a nonlinear code.

Note that the representation of the code provided by $\mathbf{G}$ is not unique. For a given generator $\mathbf{G}$, another generator $\mathbf{G}'$ can be obtained by performing row operations (nonzero linear combinations of the rows). Then an encoding operation defined by $\mathbf{c} = \mathbf{mG}'$ maps the message $\mathbf{m}$ to a codeword in $\mathcal{C}$, but it is not necessarily the same codeword that would be obtained using the generator $\mathbf{G}$.

Two important quantities must be introduced, the ratio $r \triangleq \frac{k}{n}$ defines the rate of the code, While the minimum distance $d_{min}^{\mathcal{C}}$ of a code $\mathcal{C}$ is the smallest Hamming weight (i.e. the number of non-zero components) of any codeword in $\mathcal{C}$, except the all-zero codeword,

$$d_{min}^{\mathcal{C}} \triangleq \min_{\mathbf{c} \in \mathcal{C} \setminus \{\mathbf{0}\}} w_H(\mathbf{c})$$

The number of errors, which can be corrected by the code is given by the following equation:

$$ECC = \left\lfloor \frac{d_{min}^{\mathcal{C}} - 1}{2} \right\rfloor \tag{5.4}$$

and the number of errors, which can be detected by the code:

$$EDC = d_{min}^{\mathcal{C}} - 1 \tag{5.5}$$

5.3 Soft Decoding of Linear Block Codes

Say that the receiver has completed the necessary signal processing and obtains a vector $\hat{\mathbf{w}}_l$ corresponding to the estimation of the transmitted sequence $\mathbf{c}$. The objective of the decoder is to minimize the probability of error, or equivalently, to find the codeword that maximizes the likelihood of the observations given the transmitted encoded data sequence, [15].

The decoder searches for the closest codeword $\mathbf{c} \in \mathcal{C}$, in terms of Euclidean distance. Let $\mathbf{w}_l \triangleq [w(1 + (l-1)d), w(2 + (l-1)d), ..., w(N + (l-1)d)]$ and $\mathbf{c} \triangleq [c_1, c_2, ..., c_n]$ then,

$$\hat{\mathbf{w}} = arg \min_{\mathbf{c}\in\mathcal{C}} \|\mathbf{c} - \mathbf{w}_l\|_2^2 \tag{5.6}$$

$$= arg \max_{\mathbf{c}\in\mathcal{C}} \mathbf{c}\mathbf{w}_l^T, \tag{5.7}$$

where $\hat{\mathbf{w}}_l$ is the estimation of the l-th transmitted codeword. The corresponding bit sequence $\hat{\mathbf{b}}_l$ can be extracted from $\hat{\mathbf{w}}_l$.

The full signal processing chain of the receiver is presented on Fig. 5.1.

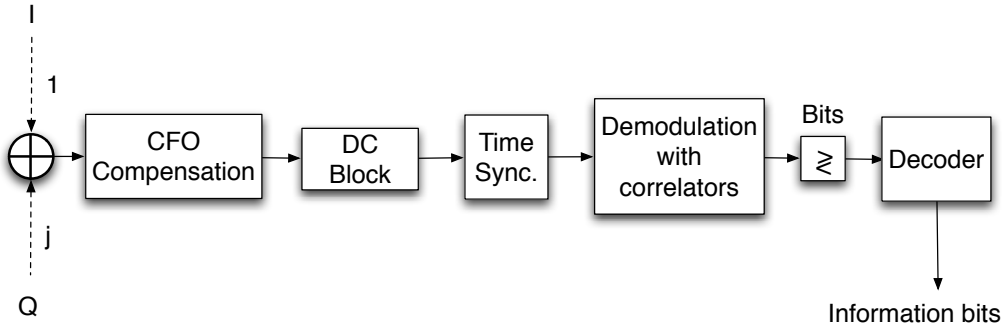Figure 5.1: Complete signal processing chain with channel decoding in bistatic backscatter radio.

5.4 Memory Organization and Encoding Algorithm

From Eq. 5.4, 5.5 it is easy to deduce that longer codes increase the reliability of the reception. But what are the costs of using longer codes? As the generation matrix and the information vector grow bigger, the computational requirements of both the encoder and the decoder grow with them. The tag utilizes an 8-bit MCU for the encoding process, which means that the computational power of the processor is limited. Thus, the length of the code must be small in order to consume less power.

However the biggest problem is not the computational power of the MCU, but its memory. The encoder must use the generation matrix in order to generate the coded bit and this matrix must be saved in the memory of the MCU. The MCU has 4 kBytes of byte-addressable SRAM memory, which the user can access with read and write privileges. But all the variables of the program are stored in this memory. This means that the generation matrices can not be stored in the internal SRAM memory.

To solve this problem the matrices are stored on the Flash memory of the MCU, since they need to be read-only. Also since, the memory is byte addressable if each bit-element of the matrix is stored in a byte position of the memory, then the memory is utilized in a bad way. To effectively utilize the memory space, each row of the generation matrix is divided in octets and each of the octets is converted to octal representation. Then it is saved in a single byte memory slot. So for Reed Muller(16, 32) the generation matrix $\mathbf{G}$ is a (16) matrix. Instead of using $16 \cdot 32 = 512$ Bytes for the generation matrix, by utilizing the aforementioned scheme, only 64 Bytes are used. With this scheme more than one generation matrices can be saved on the tag's memory, allowing the user to choose the encoding scheme used for each application.

The encoding process is performed at the tag's MCU by a multiplication of the message with the generation matrix, as described in Eq.(5.1). The output of the ADC is converted to a binary vector and it is stored in the MCU's memory. Each information bit is then multiplied and accumulated

with each row of the generation matrix and then the output of the operation
uses the modulo two operation, since a binary code is used.

Chapter 6

Conclusions

6.1 Conclusion

This work aimed in the development of a low-cost, digital sensor network, mainly for environmental sensing, utilizing the bistatic architecture. Ultra-low cost, low power and high tag density were the highest design priorities. The bistatic scatter radio system was presented which was used to create large-scale networks with extended field coverage. The individual elements of the network architecture were presented: carrier emitter and prototype scatter tags along with a software-defined reader. The complete signal model was derived for the bistatic link, for both point-to-point and multiple users scenarios, taking into account important microwave design parameters. Furthermore, the B-FSK modulation and its detection was presented. A complete analysis of the tag design is given, from the printed circuit board design to the generation of the FSK frequencies. Also, frequency division multiple access was utilized to create a network of tags divided by cells. Furthermore, channel coding was utilized to extend the up-link communication range. Linear clock code encoder and decoder were implemented, increasing the overall system's performance.

6.2 Future Work

This work only scratches the surface of the construction of a digital backscatter sensor network (BWSN). Along with [15,16,22] these are the first attempts towards a BWSN, utilizing the bistatic scatter radio link for low-power and low-cost sensor digital communication. Future work should aim to develop further the ideas presented on these works so that the bistatic link is fully

explored and utilized in its full capacity.

To eliminate the phase discontinuity, the 3rd harmonic problem, a continuous phase modulation (CPM) must be used. On these modulations the phase of the pass-band modulated signal is a continuous function of time t. Also, CPMs use modulation pulses with memory, while the classic M-FSK uses memoryless modulation pulses. The phase of the CPFSK signal changes linearly over timer and the changes that occur on the bit boundary are always $\pi/2$. CPFSK is called minimum-shift keying (MSK). MSK can be regarded as an offset quadrature phase-shift keying (QPSK) modulation of $2T$ symbol duration.

As far as the tag is concerned, more could be done on the front-end design. Important RF parameters, such as the antenna structural mode, are disregarded in the bibliography. Optimal design of the front-end will increase the communication range and decrease the energy requirements of the digital tag.

Regarding the networking aspect another scheme that could be utilized, with some major changes from its classic version is TDMA. Time division multiplexing is a very common scheme in communications. In classic TDMA the time window is divided in slots. Each time slot has a specific duration and each user is assigned to a time slot. The user can transmit only during its time slot. More sophisticated schemes utilize FDMA during the time slot, so that more than one users can communicate during the time slot. The drawback of TDMA is that in requires a down-link (sync-to-node communication) because the slot assignment is done by the sync or some other coordinator. In our case this is impossible, since the down-link does not exist.

In order for TDMA to be used, another method for assigning slots must be developed. Instead of the sync/reader to assign the slots, each tag can randomly "wake up" from its sleep mode and transmit. The probability of collision is really low, since two or more tags transmitting on the same frequencies must "wake up" simultaneously or during each other's transmission. The randomness introduced could immensely increase the number of tags in the network.

Also, the emitters used in this work utilize an embedded radio for gener-

ating the CW. The radio can also be used to construct a network consisting of the carrier emitters (See Chap. 4.2). The emitters can communicate with each other and with the reader and employ a simple TDMA scheme, granting more robustness to the network.

Furthermore, the receiver needs to be able to provide high performance in high density networks. This type of networks requires a receiver with huge amounts of computational power to process all the tags in parallel. Architectures specifically designed for this problem must be used (e.g. CUDA or FPGA based processing).

Finally, the bistatic architecture is relatively new and very little signal processing and wireless communication schemes have been employed on this problem. It is an exciting theoretical problem to work on.

Hopefully, the expansion of this work will enable ultra low-cost and large-scale environmental sensing, which was previously unfeasible with existing technologies, both due to limiting cost and relatively high energy demands.

Chapter 7

Appendix

7.1   RF Tag Schematics & Bill of Materials

Bill of Materials (for one tag):

A/A	Schematic Name	Manifucturer #	Desc	Value	Package	Quantity (for 1)
1	U1	C8051F912-GU	MCU	-	24 QSOP	1
2	Q1	BFT25A,215	Transistors RF Bipolar	-	SOT-23	1
3	LED1	SML-LX1206GW-TR	LED Green	-	1206	1
5	Y1	LFXTAL010595	Crystal 25MHz 16PF	-	Through Hole	1
6	C4	C0805C105K8RACTU	Capacitor 10V 10%	1uF	805	1
7	C5	T491A475K016AT	Capacitor Tant. 10V 10%	4.7uF	1206	1
8	C6, C1	C0805C104K3RACTU	Capacitor 25V 10%	0.1uF	805	2
9	C2, C3	C1608C0G1H220J080AA	Capacitor 25V	22pF	603	2
10	R4, R5	ERA3AEB102V	Resistor 1/8W 1%	1KOhm	603	2
11	R2	CRCW060310M0FKEA	Resistor 1/8W 1%	10MOhm	805	1
12	R1	ERJP6WF2001V	Resistor 1/8W 1%	2KOhm	805	1
13	R3	232270265471	Resistor 1/8W 1%	470Ohm	603	1
14	-	ANT-868-CW-HW-SMA	868 MHz Antenna	-	SMA	
15	-	CR2032	Coin Battery	-	-	1
16	BAT1	BS-7	Coin Battery Holder	-	Through Hole	1
17	JP6	EG1218	SPDT Switch	-	Through Hole	1
18	X1	142-0711-201	SMA	-	SMD	1
19	JP1, JP2, JP3	-	Standard Dip Connectors	-	Through Hole	1
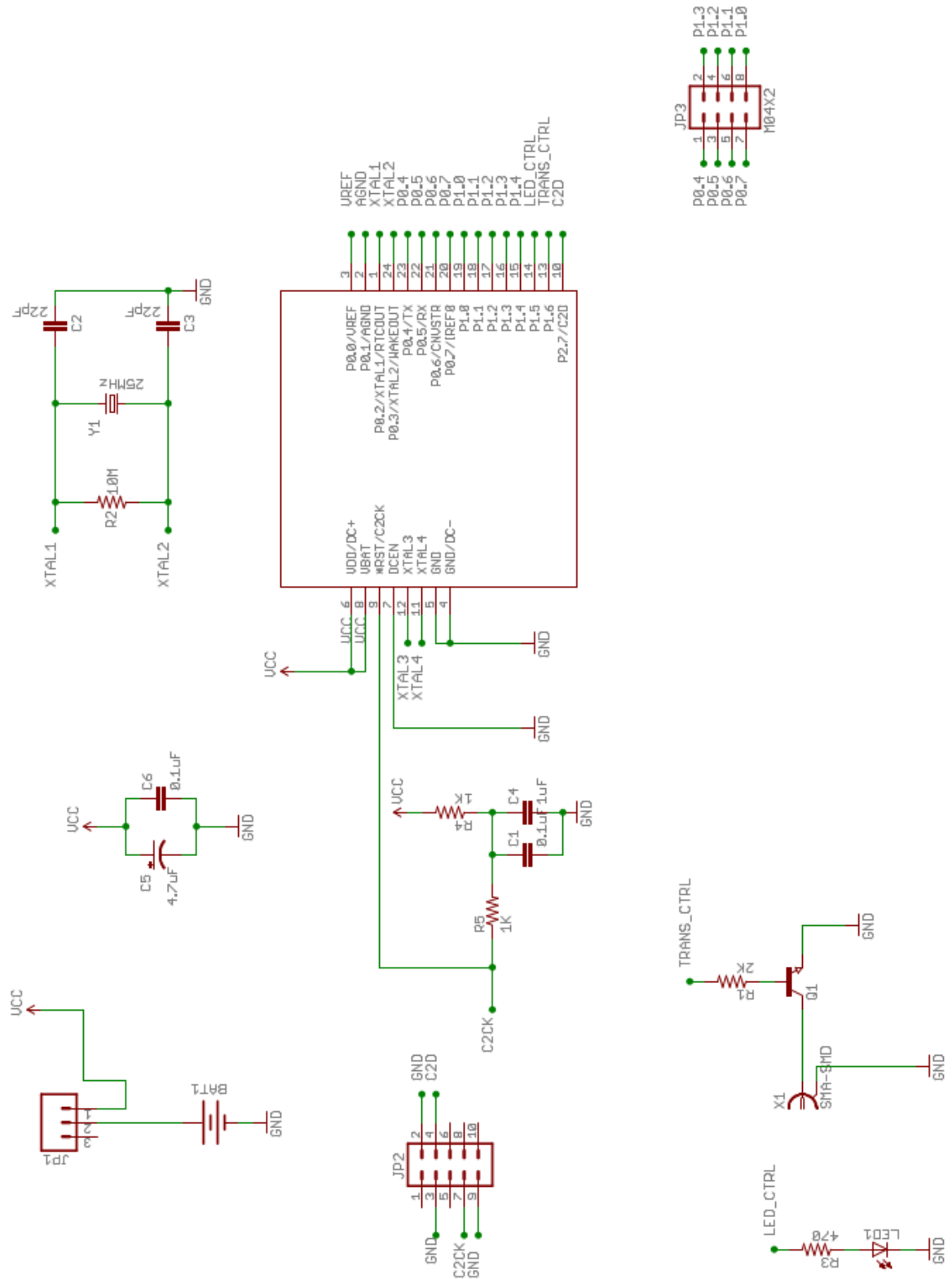
Bibliography

[1] I. F. Akyildiz, W. Su, Y. Sankarasubramaniam, and E. Cayirci, "Wireless sensor networks: a survey," *ACM Computer Networks*, vol. 38, pp. 393–422, 2002.

[2] H. Stockman, "Communication by means of reflected power," *Proc. IRE*, pp. 1196–1204, 1948.

[3] D. M. Dobkin, *The RF in RFID: Passive UHF RFID in Practice.* Newnes (Elsevier), 2008.

[4] *EPC Radio-Frequency Identity Protocols, Class-1 Generation-2 UHF RFID Protocol for Communications at 860 MHZ-960 MHZ, version 1.2.0.* EPC Global, 2008.

[5] A. Sample, D. Yeager, P. Powledge, and J. Smith, "Design of a passively-powered, programmable sensing platform for uhf rfid systems," in *IEEE Intl. Conf on RFID 2007*, Mar. 2007, pp. 149–156.

[6] E. Kampianakis, J. Kimionis, K. Tountas, C. Konstantopoulos, E. Koutroulis, and A. Bletsas, "Backscatter sensor network for extended ranges and low cost with frequency modulators: Application on wireless humidity sensing," in *Proc. IEEE Sensors*, Baltimore, USA, Nov. 2013.

[7] G. Vannucci, A. Bletsas, and D. Leigh, "A software-defined radio system for backscatter sensor networks," *IEEE Trans. Wireless Commun.*, vol. 7, no. 6, pp. 2170–2179, Jun. 2008.

[8] J. Kimionis, A. Bletsas, and J. N. Sahalos, "Design and implementation of RFID systems with software defined radio," in *Proc. IEEE EUCAP*, Prague, Czech Republic, Mar. 2012, pp. 3464–3468.

[9] J. D. Griffin and G. D. Durgin, "Complete link budgets for backscatter-radio and rfid systems," *IEEE Antennas Propagat. Mag.*, vol. 51, no. 2, pp. 11–25, Apr. 2009.

[10] D. Tse and P. Viswanath, *Fundamentals of Wireless Communication.* Cambridge University Press, 2005.

[11] D. Kim, M. A. Ingram, and J. W. Whit Smith, "Measurements of small-scale fading and path loss for long range RF tags," *IEEE Trans. Antennas Propagat.*, vol. 51, no. 8, pp. 1740–1749, Aug. 2003.

[12] G. Vannucci, A. Bletsas, and D. Leigh, "Implementing Backscatter Radio for Wireless Sensor Networks," in *Proc. IEEE Personal, Indoor and Mobile Radio Communications*, Sep. 2007, pp. 1–5.

[13] J. Kimionis, A. Bletsas, and J. N. Sahalos., "Bistatic backscatter radio for power-limited sensor networks," in *Proc. IEEE Globecom*, Atlanta, USA, Dec. 2013.

[14] A. P. A. Sample, J. Braun and J. Smith, "Photovoltaic enhanced uhf rfid tag antennas for dual purpose energy harvesting," in *IEEE Intl. Conf. on RFID*, Orlando, FL, Apr. 2011, pp. 146–153.

[15] P. N. Alevizos, "Channel coding and detection for increased range bistatic scatter radio," M.S. Thesis, TUC, 2014, mentor Aggelos Bletsas.

[16] N. H. Fasarakis, "Coherent detection and channel coding for backscatter sensor networks." M.S. Thesis, TUC, 2014, mentor Aggelos Bletsas.

[17] J. T. S. Thomas, E. Wheeler and M. Reynolds, "Quadrature amplitude modulated backscatter in passive and semipassive uhf rfid systems," in *IEEE Transactions on Microwave Theory and Techniques*, vol. 60, no. 4, Apr. 2012, pp. 1175–1182.

[18] S. Thomas and M. Reynolds, "QAM backscatter for passive UHF RFID tags," in *IEEE Intl. Conf on RFID, 2010*, Apr. 2010, pp. 210 –214.

[19] C. A. Balanis, *Antenna theory: analysis and design.* John Wiley & Sons, 2012.

[20] A. B. Antonis G. Dimitriou, John Kimionis and J. N. Sahalos, "Inventory time reduction in gen2 with single-antenna separation of fm0 rfid signals," in *IEEE International Conference on RFID Technologies and Applications (RFID-TA)*, Sitges, Barcelona Spain, Sep. 2011.

[21] J. G. Proakis and M. Salehi, *Communication Systems Engineering.* Prentice-Hall International, Inc., 2001.

[22] J. Kimionis, "Design and implementation of backscatter links with software defined radio for wireless sensor network applications," Diploma Thesis, Technical University of Crete, 2011, supervisor Aggelos Bletsas.

[23] T. S. Rappaport, *Wireless Communications: Principles and Practice.* Prentice Hall, 2002.